POLITECNICO DI TORINO

Master's Degree in Energy and Nuclear Engineering

Master's Degree Thesis

Bottom-Up and Data-Driven Modelling for Offshore Floating PV Platform

Supervisors

Prof. Giuseppe Giorgi

Prof. Emiliano Nelson Gorr

Candidate

Youssef Sdiri

July 2025

Abstract

The global shift toward renewable energy has introduced new challenges regarding space availability in Europe, particularly for solar-based systems, which have low energy density. This means they require significantly larger areas compared to traditional energy plants. Offshore floating photovoltaic (FPV) systems represent a promising solution, particularly in the Mediterranean region, where no extreme weather events have been recorded in the past forty years. Despite this, Europe still has limited FPV installations compared to other global regions. This thesis focuses on six representative European locations: Pantelleria, Gulf of Gabes, Ceuta, Jersey, Gotland, and Zadar. These locations are selected based on geographical diversity and environmental relevance, and their need for energy for both industrial and civil use. To evaluate the structural sustainability of different FPV platforms at each site, a data-driven approach (DDA) is developed, where the principal decision-making parameter is the significant wave height (H_s). Findings from this method indicate that Class 3 platforms can withstand higher H_s, while Class 2 represents the less robust structure. This study also investigates the possibility of applying seasonal removal (SR), a key operational consideration during limited periods with challenging water conditions, where the system must be dismantled and reinstalled annually. Thanks to this, for different locations, it was possible to opt for a cheaper platform type. These operations are explicitly taken into account during the techno-economic optimization analysis conducted in the thesis to ensure a more accurate and realistic long-term feasibility assessment. In parallel, a bottom-up approach (BuA) is applied to estimate the capital expenditure ($CapEx$) related to the filtered platform types found in the literature, focusing on the pontoon type. The cost breakdown includes floating, mooring, electrical substations, submarine cables, and labor, and the results show that the most robust platforms also have the highest $CapEx$. This thesis also discusses the limitations of using tracking systems on different platforms and how this affects daily and annual energy production (AEP). Other economic parameters, such as the Levelized Cost of Energy (LCOE) and Payback Time (t_{PBT}), are also analyzed and compared across the selected locations. The results show significant variations in technical, economic, and environmental performance across the selected locations. Ceuta and Pantelleria demonstrate strong economic performance, and the good results are driven by different factors: Ceuta benefits from high solar irradiance and the use of a tracking system enabled by its Class 1 configuration, while Pantelleria's profitability is due to the absence of SR and a high local electricity price, despite using a simpler fixed-tilt system. In contrast, the Gulf of Gabès faces limited revenues due to the significant impact of SR and the technical limitations of the Class 2 platform,

while Gotland shows negative returns due to environmental constraints that result in reduced energy output and high operational costs. One of the key conclusions is that the assigned platform class is a major driver of energy performance, as it determines structural flexibility and the ability to integrate tracking systems, significantly impacting yield. Moreover, a key environmental finding is that offshore FPV systems, since they are deployed in semi-isolated areas, can achieve higher tCO_2 savings, as they replace electricity from carbon-intensive sources like diesel, resulting in higher avoided emissions. Further analysis evaluates whether applying SRis economically convenient by examining the trade-offs between reduced $CapEx$, AEP and increased $OpEx$. The findings indicate that SR is only advantageous when it enables a shift from more Class 3 platforms to Class 1 configurations—where the integration of tracking systems compensates for the shorter operational period. Conversely, applying SR to downgrade from Class 1 to Class 2 often results in a net loss due to AEP and higher $OpEx$.

Acknowledgements

I would like to express my sincere gratitude to my supervisor, Prof. Giuseppe Giorgi, for his guidance and support throughout the development of this thesis. I am especially thankful to Prof. Emiliano Nelson Gorr, whose constant availability, insightful feedback, and valuable input helped me to enrich this work. I also truly appreciate the opportunity to have a place at the MORE Center during my time in Torino, which provided not just a space to work, but a motivating and supportive environment for my research. Thank you again both for your help, patience, and continued support throughout this journey — and beyond.

Desidero esprimere la mia sincera gratitudine al mio supervisore, il Prof. Giuseppe Giorgi, per la sua guida e il suo supporto durante lo sviluppo di questa tesi. Un ringraziamento speciale va al Prof. Emiliano Nelson Gorr, la cui costante disponibilità, i feedback preziosi e i numerosi suggerimenti hanno arricchito notevolmente questo lavoro. Apprezzo profondamente anche l'opportunità di avere uno spazio presso il MORE Center durante la mia permanenza a Torino, che mi ha offerto non solo un luogo dove lavorare, ma anche un ambiente stimolante e di supporto per la mia ricerca. Grazie ancora ad entrambi per l'aiuto, la pazienza e il costante supporto lungo questo percorso — e oltre.

Table of Contents

List of Tables

List of Figures

Acronyms

AC Alternating Current

AEP annual energy production

$\beta_{\mathbf{opt}}$ Optimal tilt angle [°]

$\mathbf{B_t}$ Discounted net cash flow at year t

BuA Bottom-up Approach

$CapEx$ Capital Expenditure

$\mathbf{C_{boat}}$ Charter cost of jack-up vessel (daily/hourly)

$C_{\mathbf{chain}}$ Cost of the mooring chain

$\mathbf{C_{divers}}$ Cost of divers (per unit of time)

$\mathbf{C_{diesel}}$ Local diesel price [€/L]

$\mathbf{C_{diesel\text{-}kWh}}$ Cost per kWh of electricity generated by diesel

$C_{\mathbf{drag}}$ Cost of the drag-embedment anchor

$\mathbf{C_{grid}}$ Local household electricity price [€/kWh]

$C_{\mathbf{mooring}}$ Total cost of the mooring system

$C_{\mathbf{panel}}$ Cost per PV panel [€]

$\mathbf{C_{platform}}$ Total platform cost

$C_{\mathbf{PV}}$ Total cost of PV modules [€]

$C_{\mathbf{cables}}$ Cost of the submarine cables [€]

$C_{\mathbf{substation}}$ Cost of the electrical substation [€]

$\mathbf{C_{workers}}$ Cost of workers (per unit of time)

$\mathbf{C_{manufacturing}}$ Manufacturing and assembly cost

$\mathbf{C_{kWh}}$ Cost of energy per kilowatt-hour

d Day index

DDA Data-Driven Approach

DC Direct Current

δ Annual degradation rate of the PV system

δ Solar declination angle [°]

$d_{\mathbf{coast}}$ Distance from the shore [km]

d(x, y) Distance from installation site to shore based on spatial coordinates

$EF_{\mathbf{avg}}$ Average emission factor [kgCO_2/MWh]

$EF_{\mathbf{diesel}}$ Emission factor of the diesel generator [kgCO_2/MWh]

$EF_{\mathbf{grid}}$ Emission factor of the grid [kgCO_2/MWh]

$\eta_{\mathbf{diesel}}$ Fuel consumption rate of diesel generator [L/kWh]

E_y Annual energy output in year y

FPV Floating Photovoltaics

γ Correction factor accounting for floating cooling effects

$\mathbf{G^{daily}_{d}}$ Total daily irradiance for day d

$\mathbf{\bar{G}_{d,h}}$ Mean irradiance at hour h on day d over N years

$\mathbf{G_{y,d,h}}$ Irradiance value in W/m^2 for year y, day d, and hour h

h Hour index

$\mathbf{H_{1/3}}$ Average height of the highest one-third of waves

H_d Sea depth

HDPE High-Density Polyethylene

$\mathbf{H_j}$ Wave height of the j-th wave

H_s Significant Wave Height

$\mathbf{H_{s,inside}}$ Significant wave height inside the protected area

$\mathbf{H_{s,offshore}}$ Offshore significant wave height

I Initial investment cost

$\mathbf{K_t}$ Transmission coefficient

$l_{\mathbf{chain}}$ Length of the mooring chain

LCOE Levelized Cost of Energy

MBL Minimum Breaking Load

$\mathbf{MC_t}$ Maintenance cost at year t

N Total number of years used for averaging

$\mathbf{n_{FPV}}$ Total number of floating PV units to be installed

$\mathbf{n_{FPV\_pertrip}}$ Number of FPV units transported and deployed per trip

i Nominal discount rate

NPV Net Present Value

$OpEx$ Capital Expenditure

$t_{\mathbf{PBT}}$ Payback Time

$P_{\mathbf{corr},h}$ Corrected energy production at hour h, accounting for floating cooling effects

ϕ Latitude of the location [°]

$\overline{P}_h$ Average power output at hour h over N years

$P_{h,y}$ Power output at hour h of year y

P_n Nominal power of the FPV system [MW]

$P_{\mathbf{panel}}$ Nominal power of a single PV panel [W]

PV Photovoltaics

PVGIS Photovoltaic Geographical Information System

$\mathbf{Q_i}$ Quantity of material i

RES Renewable Energy Sources

SR Seasonal Removal

$\mathbf{tCO_2}$ Tons of Carbon Dioxide Equivalent

TdA Top-down Approach

θ_s Solar elevation angle [°]

$\mathbf{T_{install}}$ Installation time per FPV unit

u East–west (zonal) component of wind

$\mathbf{u_i}$ Unit cost of material i

v North–south (meridional) component of wind

$\mathbf{v_{boat}}$ Speed of jack-up vessel during transport and installation

W Wind speed

$\mathbf{x_{99.5}}$ 99th percentile value

y Year index

ω Hour angle [°]

DS Design Structure

Chapter 1

Introduction

Addressing climate change is a cornerstone of international policies, particularly within Europe, where reducing greenhouse gas emissions is crucial to meeting the ambitious targets outlined in the European Union's Green Deal, which includes a goal of achieving a 32% renewable energy share by 2030 [1]. As global demand for renewable energy continues to increase, there has been significant innovation in photovoltaic (PV) technologies. While land-based PV systems have become widespread, floating photovoltaic (FPV) systems —especially those deployed on inland water bodies such as lakes and reservoirs—are gaining attention as a valid alternative [2, 3]. However, the potential of FPV systems in coastal and offshore environments remains largely unexplored, despite the advantages they offer. PV systems traditionally suffer from low energy density production, which means they need a large portion of land compared to other sources of energy, which becomes problematic in areas with scarce and expensive land—such as small islands or densely populated regions [4]. So, from here we have one of the main key benefits of FPV systems, that is, reduction in land use; another advantage is given by the mitigation of water evaporation in lakes and water reservoirs. Another point that is interesting also in off-shore FPV systems is the potentially increased energy efficiency through natural water cooling effects, given by the lower operational temperatures of PV, that decrease the thermal losses and degradation over the life time of the system [5].

While FPV systems have been successfully deployed in inland water bodies[2, 3], their application in offshore environments remains limited. This is primarily due to harsher conditions such as strong winds and large waves. Despite this, offshore systems offer significant advantages, including abundant space, high solar irradiance, and proximity to urban centers, with over 40% of the global population living within 100 km of coastlines [6]. However, at the moment, only a small fraction of installations have been placed offshore. Moreover, existing literature has largely concentrated on systems installed in continental water bodies and hydropower

reservoirs, rather than truly marine environments. For example, several studies have assessed the integration of FPV with inland water resources, including in Spain and Italy, or conducted techno-economic analyses for systems installed on lakes and reservoirs [2, 3]. In the literature, there is also a lack of detailed cost breakdowns: most studies rely on a top-down approach (TdA) to estimate the capital cost ($CapEx$) of the FPV system —typically between 30% and 40%—compared to ground-mounted system [7, 8]. These methods don't provide enough details about the choice of materials for the floating structure, mooring layout, or installation challenges specific to marine environments. However, in this study, a bottom-up approach (BuA) is used to break down the cost component by component, based on actual design and site conditions.

Among the few studies using the BuA, [9] carried out a detailed techno-economic analysis of a Class 1 floating platform. However, their work is limited to a fixed nominal power and doesn't examine how economic metrics like $CapEx$, levelized cost of energy (LCOE), or net present values (NPV) might change with different system sizes. As a result, questions about the scalability and adaptability of FPV cost structures are still largely unanswered in the existing literature. Another key innovation of this study is the use of a data-driven approach (DDA) to determine the structural performance limits of different FPV platforms. To date, no existing study has systematically analyzed the robustness of these structures based on real-world data. By examining significant wave height (H_s) data from locations where these platform types have already been deployed, this work derives the maximum sea conditions each platform can withstand, offering valuable insights into their operational limits. In terms of energy production, the structural layout of each platform is also taken into consideration, as it can significantly influence system performance. For instance, some platforms are compatible with solar tracking systems, while others are not, resulting in notable differences in energy yield and, consequently, in key economic indicators such as the LCOE and Payback Time (t_{PBT}). The findings of this study aim to support the development of offshore FPV systems, offering a clear comparison between different platform configurations and providing a solid basis for future investment and implementation strategies. In addition, a parametric tool with a user-friendly dashboard interface has been developed as part of this work. The tool allows users to input key parameters—such as the selected location and the nominal power of the desired system—and receive recommendations on the most suitable platform configuration for that site. It also provides performance metrics, including estimated energy production, and key economic indicators such as the LCOE, t_{PBT}, $CapEx$, and the $OpEx$.

The following chapters of this thesis are organized as follows:

- **Chapter 2**: presents the current state of the art in FPV applications, including technological components such as PV modules, tracking systems, and mooring strategies, as well as the structural classification of floating platforms.

- **Chapter 3**: discusses the criteria for selecting the case study locations and introduces the six selected sites, reflecting a wide range of maritime and climatic conditions across Europe and the Mediterranean.
- **Chapter 4**: details the DDA for the platform classification, using the H_s to assign platform classes and assess seasonal removal (SR) feasibility.
- **Chapter 5**: focuses on energy production analysis, evaluating solar irradiance, optimal orientation of PV modules, and the effect of water cooling on energy yield.
- **Chapter 6**: presents the BuA estimation methodology, breaking down the costs for different platform classes and associated components.
- **Chapter 7**: integrates the energy, environmental, and economic assessments, including metrics such as LCOE, NPV, t_{PBT}, and the tonnes of carbon dioxide $\mathrm{tCO_2}$) emissions avoided.
- **Chapter 8** discusses and interprets the results obtained from the previously described methodologies, highlighting the performance differences between the various locations and FPV systems from an economic, environmental, and financial perspective. It also assesses the overall impact of SR on energy yield, and consequently, on the economic feasibility of the system.
- **Chapter 9** outlines future improvements to the methodology, including addressing current limitations and suggesting directions for further research and development.
- **Chapter 10** summarizes the main results of the thesis.

Chapter 2

State of the Art in Floating PV Applications

A FPV system is usually composed of: modules to capture the solar energy, floating structures to provide buoyancy, a structure that supports the solar panels, a mooring system that prevents uncontrolled movement of the whole system, and the electrical components need to integrate the power system to the grid [10]. As illustrated in Fig. 2.1, the concept of FPV systems is very similar to the traditional on-shore PV systems, the only difference is that the PV modules are mounted on the floating structure [4].

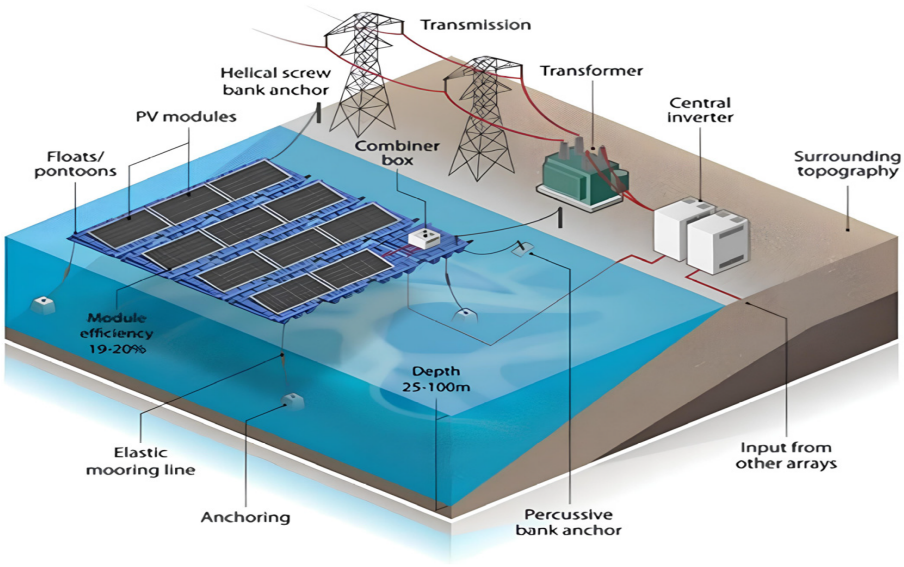

Figure 2.1: Conceptual layout of an FPV installation [2]

2.1 PV module

The PV modules used in floating systems are similar to those in land-based installations. They consist of solar cells that utilize light-absorbing materials to capture photons and generate free electrons through the photovoltaic effect [11]. Standard crystalline solar PV modules have been the most used for commercial large-scale FPV plants, but in some cases, have been used with thin-film modules . These types of modules have the advantage of being flexible, which is beneficial for enduring the wave loads in marine applications [12], but they have not yet been commercialized. In the marine environment, the modules need to resist higher loads and withstand saltwater corrosion [13], because this environment can accelerate the degradation, and the soiling loss: due to dust accumulation, bird dropping and other particles that covers the surface of the PV module, decreasing the energy production [14]. Unfortunately, the energy loss production is not the only problem; these types of soiling loss can shade the PV and form hotspots: high temperature locations that can permanently damage the modules [13]. The loss of productivity due to the panel degradation is considered by including a decrease factor equal to 2% per year [9]. There is also the option to exploit bifacial modules: modules that can convert light arriving on both the front, so the second face of the module exploit the albedo coming from the ground, in the case of FPV applications, this technology is not that beneficial due to the low albedo of water compared to the ground [14]. But installing reflectors on the floats can increase the albedo, and therefore the yields of the bifacial module would be 13.5% times greater of the monofacial ones [15].

2.2 Tracking Systems

The tracking system in FPV systems can be applied to improve the energy yield by adding a mobile structure that supports the PV modules [10]. We can have both: vertical and horizontal axis tracking systems, the first one can be implemented in different ways, for example, as a submerged structure that rotates the floating following the path of the sun, while for the horizontal axis we need just to make the frame structure with a variable tilt angle [16]. But it depends on the pontoon-type that we are using, it will be seen that some configurations allow the installation of just horizontal panels, without the possibility of adjusting the tilt angle. It has been proven that a dual-axis system can increase the energy yield by almost 30%, but on the other hand, we can have a cost increase of almost 100% [17]. This significant increase is attributed to the advanced mechanical and control systems for dual-axis tracking , leading to substantially higher initial investments.

2.3 Electrical components

For the transport and transformation of the electricity from the FPV to the grid, we need an array of cables and electrical components. The cables can be installed under the water or kept above, but in both cases, we need to make them waterproof, and also in the design of the cables, the high level of UV radiation and the great temperature fluctuations need to be considered [10]. The use of a DC-DC converter is needed to reach the needed voltage, due to the intermittent nature of solar power plants. Then an inverter that converts DC to AC at the desired frequencies to be then put in the grid. These components can be installed directly onshore or the floating system. In the first case, we will have an on-shore substations, that do the needed transformations, before putting the current in the grid: so the export cable that comes from the system will be DC, while if all the electrical components are kept on the platform, it will have an AC cable that connects directly to the grid [18]. When it is possible is always better to go for an on-shore substation, as doing so will be easier to install and cheaper $OpEx$ when needed, since the most critical components are on-shore.

2.4 Mooring and anchoring system

The mooring system is essential to restrict the free movement of the floating structure, counteracting environmental forces such as wind, waves, and currents. Its primary function is to prevent damage and collisions between floating components[9, 7]. In marine applications, mooring lines typically consist of steel chains, while anchors are commonly constructed from concrete piles [18, 19]. Mooring systems can be classified into four main categories[10]:

- Catenary mooring: Consists of chains whose own weight creates a force that offers flexibility and stability to the moored structure.
- Compliant mooring: A variation of catenary mooring, which uses floats and weights to modify and adjust the arrangement of mooring lines.
- Taut mooring: keep the lines under constant tension, using extra buoyancy to hold everything in place.
- Rigid mooring uses solid structural components fixed to the seabed. It allows the platform to move up and down with the waves but limits horizontal movements like drifting or swaying.

2.5 Design and classification of the floating structure

A large number of projects in the last few years have led to the development of different floating structures, with different designs and materials, based on the site conditions. There are two main classifications, one is given by DNV Recommended Practice document DNVGL-RP-0584 [20], where there are three main types:

- Pure float: this type of FPV array has the PV modules that are mounted directly onto the floats. The floating structure is designed with built-in mechanisms, such as clamps or fixings, to secure the PV equipment in place. Each float in a pure floats system can be designed to support multiple PV modules.
- Membranes: In this type of FPV array, the PV equipment is mounted on a reinforced membrane, which is supported by additional structures, such as tubular rings, to provide buoyancy. The combination of the reinforced membrane and tubular ring serves as both the float and the floating structure. The tubular ring may also support components like combiner boxes.
- Taut mooring: keep the lines under constant tension, using extra buoyancy to hold everything in place.
- Rigid mooring uses solid structural components fixed to the seabed. It allows the platform to move up and down with the waves but limits horizontal movements like drifting or swaying.

There is another classification for FPV, which is frequently cited in the literature [9, 10, 14], and is always based on their structural arrangement. A first division is based on the relative position of the PV modules to the water surface. When modules are placed directly at the waterline, they benefit from better cooling, which can potentially improve their efficiency. However, this configuration also increases their exposure to the stress caused by the wave forces. FPV systems can therefore be categorized as either superficial, where modules are mounted directly above the water, or pontoon-type, where the modules are supported by an elevated floating platform that acts as an intermediary structure [10].

2.5.1 Pontoon-type

The main characteristic of the pontoon type is the presence of a raft to give stability to the solar modules, and there are three different main classes based on the different existing design [10].

Class 1

The earliest FPV structures are categorized as Class 1, consisting of rafts made with parallel HDPE cylinders as floats and supported by steel, aluminum, or fiber-reinforced plastic components. These designs have minimal contact with the water and can easily accommodate features like single-axis tracking systems [14, 10]. While robust and versatile, Class 1 systems are generally more expensive compared to other alternatives [10]. The first large-scale, non-experimental FPV plant belongs to this category, and it had a nominal power of 200kW and was installed in fresh water in Suvareto, Italy [14]. In marine environments, Class 1 systems have been installed in locations with moderate wave conditions [10]. However, they face challenges, such as excessive flexural stress from incoming waves, which can be addressed using hinged structural elements [21]. One example, the Swimsol SolarSea system, is designed for marine conditions, using aligned floaters instead of cylindrical floats. The floaters are connected by an aluminum truss that raises the panels above the water to prevent saltwater splashes [10].

Class 2

Class 2 FPV systems were first introduced by Ciel & Terre in 2011 under the commercial name Hydrelio [22, 10]. With this design is each PV panel is supported by a single float with built-in rails. These floats can also house electrical components, serve as perimeter barriers, or create walkways. The floats are connected via pins, eliminating the need for an additional supporting structure [14]. This makes Class 2 systems more affordable than Class 1, though they are less customizable, limiting the integration of efficiency-enhancing technologies. Class 2 systems have a larger contact surface with the water, which can lead to faster material degradation and a higher environmental impact [10]. These systems are mostly used in freshwater applications and can resist waves up to 1 meter, making them not ideal for open-sea environments. However, due to their cost advantages, several companies have adopted similar designs, and deployments in marine conditions have been made. A notable example is a nearshore FPV plant built in the Persian Gulf, where the site was naturally sheltered, and bifacial solar modules were used to withstand the constant salt spray [23]. Chenya Energy also constructed a Class 2 FPV plant off the coast of Taiwan, which became the world's largest offshore solar plant at the time [24, 10]. Despite these advancements, Class 2 designs may still face challenges in fully offshore environments.

Class 3

Class 3 FPV systems consist of floats assembled to form a large floating platform or "island", where the PV modules and electrical components are installed separately.

These platforms are typically rigid and walkable, eliminating the need for catwalks. This design results in a stable and safe structure, making maintenance easier, and this makes the cost higher compared to other types [10, 14]. This type of floating platform has a variety of designs: in some instances, the usual HDPE floats have been replaced by concrete platforms. Thanks to the robust design, the Class 3 systems are suitable for marine environments TThe world's first high-wave FPV is installed by the company Oceans of Energy in the Dutch North Sea, and falls into this category, having resisted storms with waves up to 10 meters [25].

2.5.2 Superficial

This category has the characteristics of having a thin layer of water covering the PV modules: this has the advantage of increasing the cooling effect and to mitigates the effect of wind loads on the modules, while on the other hand we have direct loads from the waves and the increase of corrosion due to the salinity of the sea water [26]. In [10] two different strategies have been proposed to withstand these environmental conditions: the rigid and the flexible approach.

Rigid

A rigid FPV plant has been proposed by, and it's said that it can submerge up to 2 meters and to be able to withstand the wave loads. This is because the wave-induced velocity of water decreases with water depth [10]. But the light that can reach the modules will be much lower, due to the light absorbed by the water, with the consequence of reduced energy production by the system.

Flexible

The flexible FPV strategy includes two main approaches: Thin-film flexible modules, typically made from amorphous silicon, and the crystalline silicon modules supported with flexible foam [27] . Thin-film modules are lightweight, use minimal materials, and offer advantages like natural cooling, fewer components, better wave resistance, and lower mooring system costs due to reduced hydrodynamic interaction [10]. However, they cannot be tilted or tracked, and wave motion may affect module orientation, lowering efficiency compared to pontoon-based systems. Even if they are not submerged, the closed distance from the water enhances cooling, potentially increasing yield by 5% times over pontoon systems. Ocean Sun is testing systems in the Canary Islands and South Korea [28]. A Dutch company is also testing a 20-kW pilot system in the Port of Rotterdam, aiming to scale it up to 5 MW on the North Sea [29, 10].

Chapter 3

Location selection criteria

3.1 Why The Mediterranean Sea and Europe

The Mediterranean Sea presents an attractive location for the deployment of FPV systems due to several favourable environmental and climatic conditions. Ensuring the safety and reliability of FPV systems under varying wave and wind conditions is crucial for their successful deployment and long-term operation. In this paragraph, we will compare it to the rest of the world. To assess the wind and wave conditions, David Firnando Silalahi et al. [30] has utilized ERA5 reanalysis data from the European Centre for Medium-Range Weather Forecasts. ERA5 reanalysis is a comprehensive global climate and weather reanalysis tool that provides hourly data on wind speeds (W) and H_s over 40 years (1980-2020) [31]. The ERA5 dataset includes W data arranged in an 11 km $\times$ 11 km grid format. This dataset provides the u-component and v-component of Ws at 10 meters above water level, representing the horizontal speed of air moving eastward and northward, respectively. W was calculated hourly using the following formula:

$$W = \sqrt{u^2 + v^2} \tag{3.1}$$

In the map in fig 3.1 , we have marked in red the maritime areas that have experienced H_s than 10m and W larger than 20m/s at sometimes over the last 40 years.

We can see that the Mediterranean is one of the five main areas where we didn't have any extreme events and in the last 40 years, together with Southeast Asia, the Red Sea, Equatorial Africa, and South America. Now, by focusing on the different Mediterranean regions, we can see, according to the work of Francesco Barbariol et al. [32], we have the median wave heights through the year, as depicted in Fig. 3.2.

The median H_s in the Mediterranean varies by season. During winter (November to March), the largest waves, up to 1.5 meters, occur in the western and southern

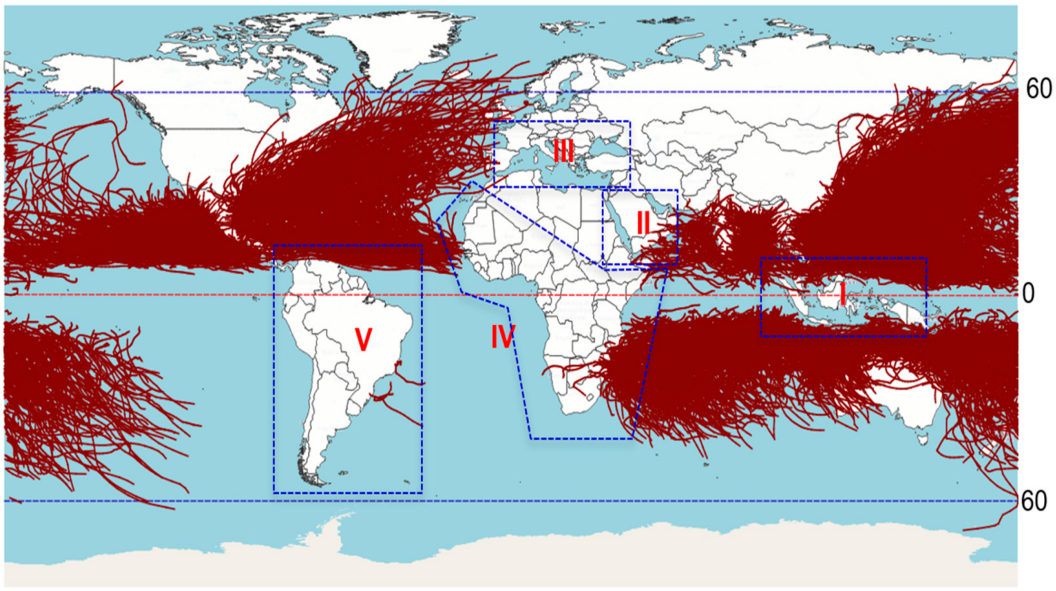

Figure 3.1: Historical Storm Paths [30]

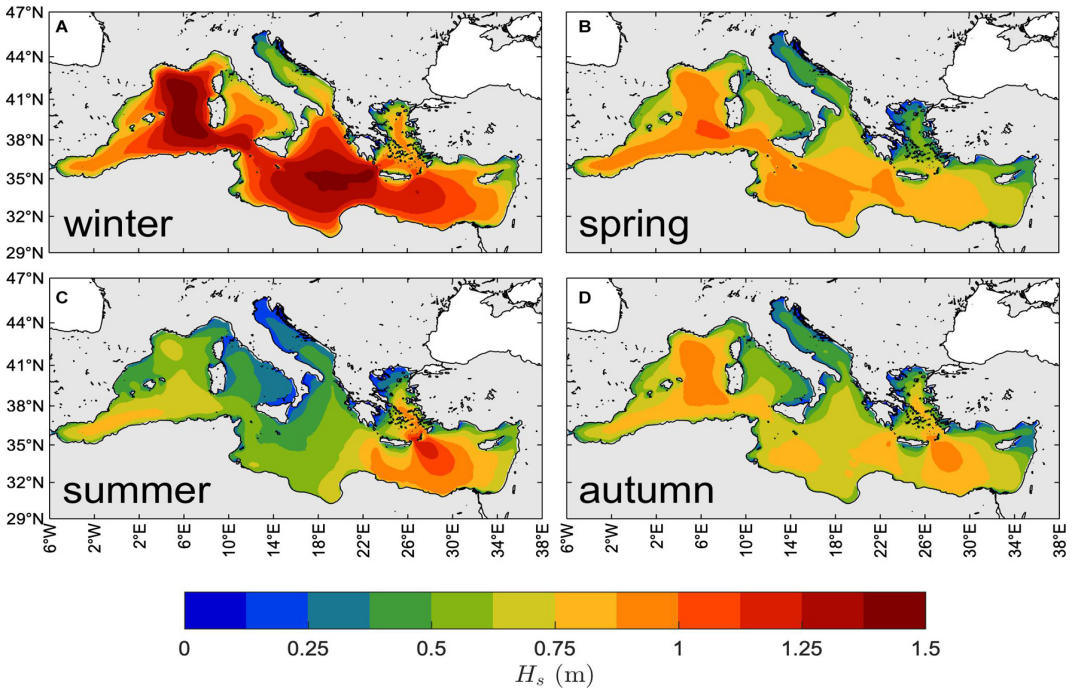

Figure 3.2: Geographical distiribution of the median wave height [32]

parts of the sea due to stronger winds, while in spring (April and May) and autumn (September and October) we have that the wave patterns are similar, with typical heights around 1 meter, particularly energetic in the western basin near the Sardinian Sea. In summer (June to August), the median H_s are very low, and the whole region is calm. For extreme wave conditions (99th percentile), we can see the variations in Fig. 3.3.

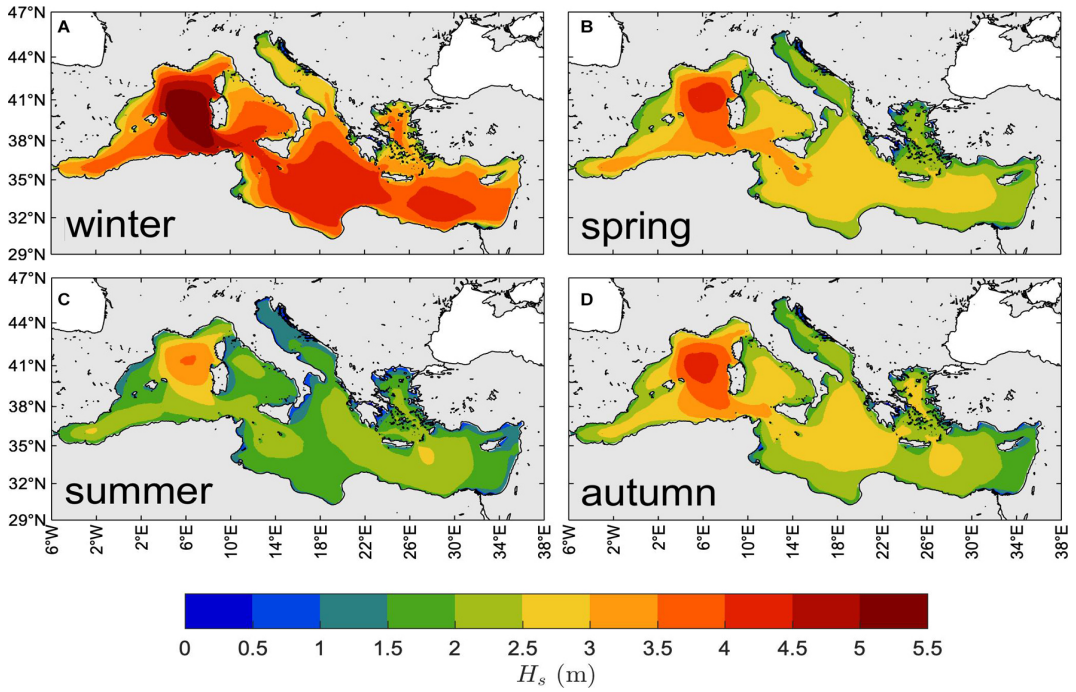

Figure 3.3: Geographical Distribution of the 99th precentile [32]

The Gulf of Lyon and the Sardinian Sea experience the most severe H_s, reaching up to 5.5 meters in winter and 4.0 meters in summer. H_s are also notable in the Ionian and Levantine Seas, influenced by various wind patterns such as the Sirocco, which generates high waves along the eastern coastlines. But by keeping focus on the extreme events during the winter season, we have several regions having comparatively calmer conditions:

- Adriatic Sea: Particularly along the Croatian coast and the northern areas of the Adriatic Sea.

- Gulf of Gebes (Tunisian East Coast): This region experiences calmer seas in winter due to its location away from the main paths of the more severe winter storms that affect the western Mediterranean.

- Aegean Sea (Greek and Turkish Coasts): Especially along the Aegean Sea and parts of the Levantine Basin

Wave conditions are not the only critical factor when selecting suitable locations for offshore FPV deployment—bathymetry also plays a key role. By consulting the bathymetry map generated through EMODnet [33] in Fig. 3.4, it is possible to observe that the Mediterranean Sea is generally shallow, with an average depth of 1500 m, it reaches a maximum depth of 5150 m off the southern coast of Greece.

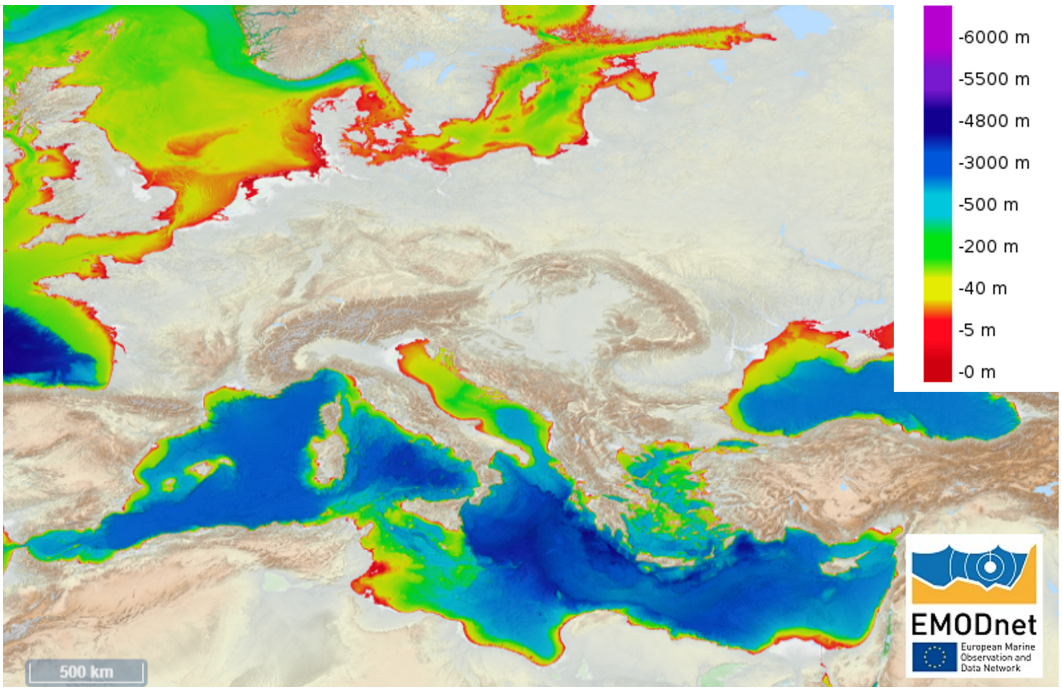

Figure 3.4: Depth in the Mediteranean See [33]

The Aegean Sea, with its varied depths ranging from shallow coastal waters to deep basins exceeding 2,500 meters, contrasts sharply with the northern Adriatic Sea, which averages around 250 meters in depth with its extensive continental shelf. For FPV systems, the shallow and stable waters of the northern Adriatic are more favourable due to easier installation, mooring, and maintenance, whereas the Aegean Sea's deeper areas may require advanced technology and incur higher costs for stable anchoring and maintenance of FPV systems. That is why we decided to exclude the Aegean Sea from our sites of interest. While the Gulf of Gabes and the northern Adriatic Sea, with their shallow waters never exceeding 50 meters, facilitate easy installation and anchoring of FPV systems. Since in our studies we are interested in diverse climatic and maritime conditions, we will also focus our interests on less stable regions.

3.2 Ceuta

Ceuta is an autonomous city located on the north coast of Africa, Fig. 3.5, bordered by Morocco and situated along the Strait of Gibraltar. This strategic location provides Ceuta with unique geopolitical significance. The city covers an area of about 18.5 square kilometers and has a population of approximately 85,000 residents [34]. Ceuta enjoys a Mediterranean climate characterized by mild, wet winters and hot, dry summers, which is conducive to solar energy projects due to high solar irradiance. Given its strategic location and climatic conditions, there is significant potential for integrating RESs to meet Ceuta's energy needs sustainably. Ceuta benefits from high solar irradiance, making it a prime candidate for solar energy projects. The abundant sunlight throughout the year can be harnessed to support various energy needs, reducing the city's dependence on non-RESs and lowering greenhouse gas emissions. Enhancing energy efficiency and focusing on renewable energy integration can help Ceuta address its growing energy demand, particularly during the summer months when consumption peaks. Ensuring a reliable supply of freshwater is also crucial for both residents and the tourism industry. By leveraging its geographic and climatic advantages, Ceuta can develop innovative solutions to enhance water and energy security, contributing to a more sustainable future.

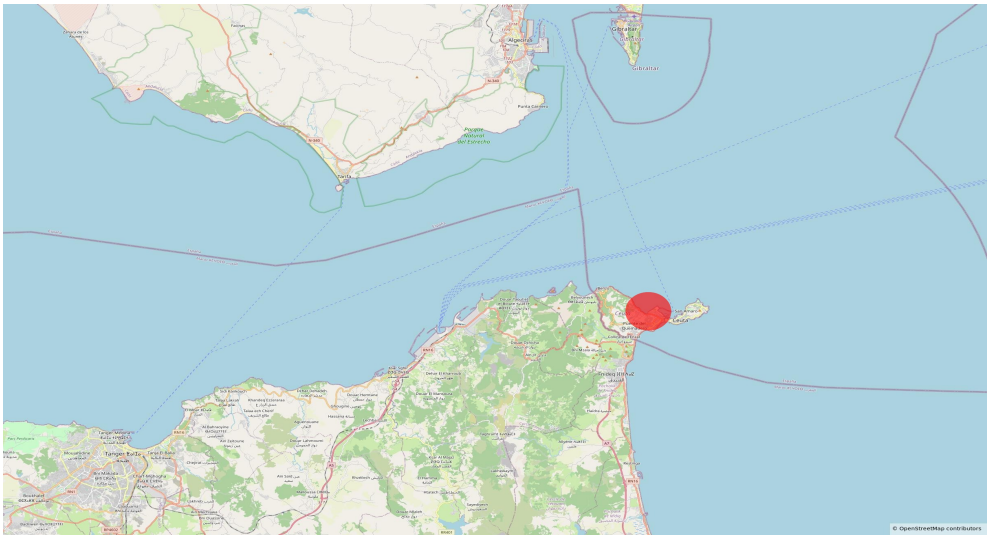

Figure 3.5: Ceuta: Proposed FPV grid connection site along the coastline. [35]

Ceuta relies heavily on its desalination plant (DS) to meet its water demand. With an installed capacity of 30,137 cubic meters per day, the plant produces an annual desalinated volume of 8.4 hm^3. Given the city's total annual water demand of 9.5 hm^3, the DS covers approximately 88% of the water needs. This high desalinated-to-demand ratio underscores the critical role of desalination in

ensuring a reliable freshwater supply for Ceuta [36]. The DS in Ceuta is located at the coordinates [35.898331, -5.340907], situated inland. This strategic location in a re-entrant ensures that the plant is protected from the heavy maritime traffic passing through the Strait of Gibraltar, minimizing potential disruptions and operational issues related to sea traffic.

Figure 3.6: Ceuta Desalination Plant [35]

By analysing the bathymetry of area, it is possible to observe that the seabed never goes deeper than 25 meters, making it easy to install the mooring system and since the main root of ships is far from this area, we are free to install the system in the surrounding area without constraints.

3.3 Pantelleria

The island of Pantelleria, with the following coordinates [36.780, 11.953], is situated in the Strait of Sicily between Italy and Tunisia, and serves as a strategic point approximately 100 km southwest of Sicily [37]. The island relies heavily on a diesel power plant for its energy needs, generating 39.0 GWh annually, supplemented by 0.5 GWh from distributed PV systems on rooftops. This dependence on diesel generators results in high import costs, as fossil fuels are transported from the mainland [38].

The island's water supply relies on energy-intensive desalination processes, consuming about 3.7 GWh of electricity per year. This interdependence between water and energy systems underscores the potential benefits of integrating FPV systems. By exploiting more solar energy, the island could reduce its reliance

on costly diesel imports, optimize the desalination process, and improve overall sustainability. It has also proven that there is an alignment between the peak water production/electricity demand and high solar irradiance[38], further supporting the feasibility of this renewable energy solution.

Concerning desalination, there are currently two reverse osmosis plants on Pantelleria island: one comprises 4 desalination modules with a production capacity of 1200 m3/day each, while the other one has a single module for 1000 m3/day. The two plants are located in Maggiuluvedi and Sataria [39].

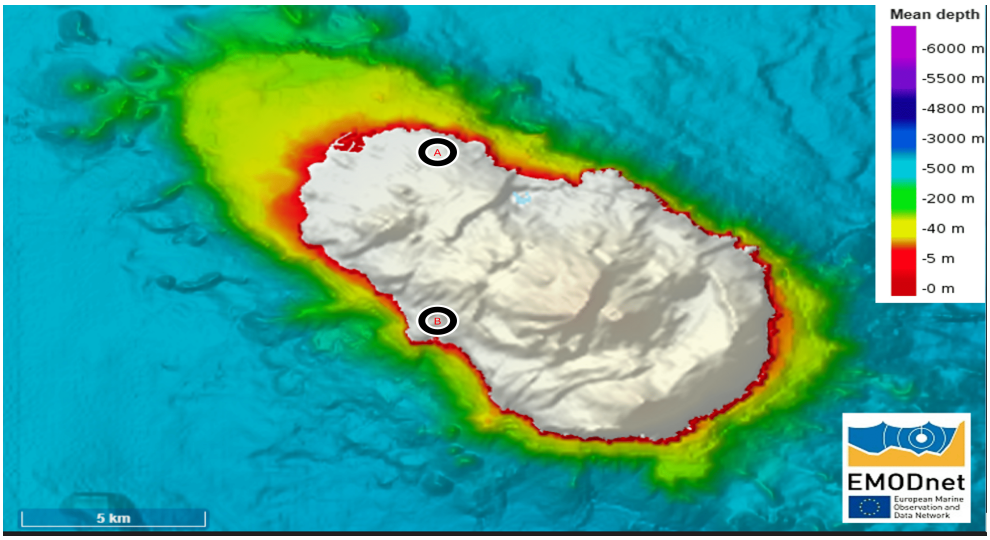

Figure 3.7: Bathymetric map of the area surrounding Pantelleria Island, illustrating depth contours critical for FPV site assessment. [33]

3.4 Zadar

Zadar is a historic city located on the Adriatic Sea in Croatia, approximately 300 kilometers southwest of the capital, Zagreb. It covers an area of about 25 square kilometers and has a population of approximately 75,000 residents. Zadar benefits from a Mediterranean climate with high solar irradiance, making it an ideal candidate for solar energy projects. This abundant sunlight makes Zadar well-suited for initiatives focused on renewable energy and sustainability [40].

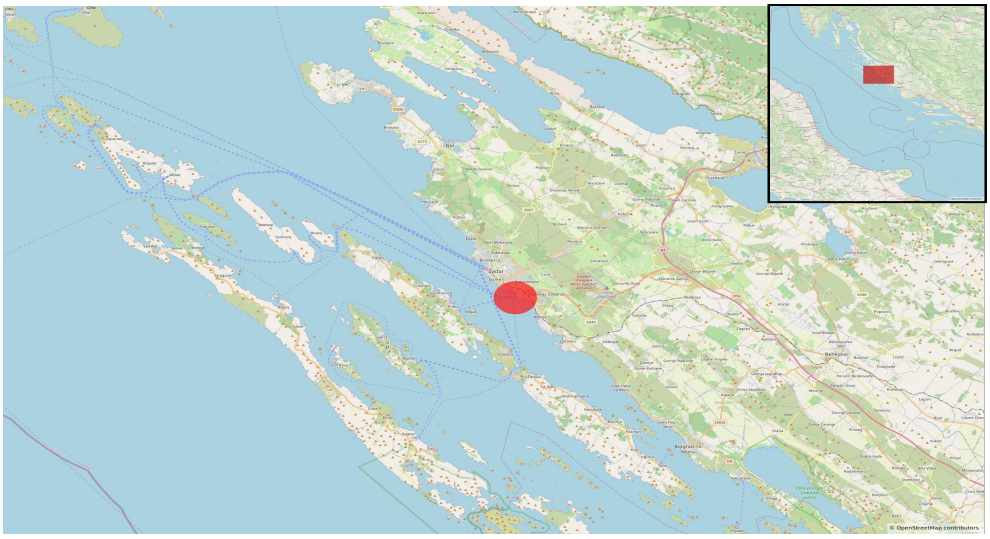

Figure 3.8: Zadar: Proposed FPV grid connection site along the coastline. [35]

The Port of Zadar is the largest cruise port in Croatia and serves several anchor clients in the dry bulk, liquid bulk, and general cargo sectors. In 2015, it welcomed 2 million ferry passengers on both domestic and international routes, making it the country's second-largest passenger port after Split. One of the main trends in energy and environment policy is the adaptation of green policies. The reduction of greenhouse gas emissions is becoming a top priority for the port and transport sectors, as new regulations are being drafted at both the EU and international levels. Considering the Green Port Concept, the Port of Zadar should aim to become a "green" port to increase its focus on environmental sustainability. This involves implementing green policies and practices to reduce emissions and enhance sustainability. By leveraging its high solar irradiance, Zadar can integrate solar energy projects to support these green initiatives, positioning the port as a leader in environmental stewardship and sustainable development [40].

3.5 Gulf of Gabes

The Gulf of Gabès, located off southeastern Tunisia, spans about 70 kilometers and is characterized by shallow waters and extensive tidal flats. It has a Mediterranean climate with hot, dry summers and mild, wet winters, benefiting from high solar irradiance. The main cities along the Gulf are Gabès and Sfax, which support a significant population. These coastal cities play a crucial role in the region's dynamics and development.

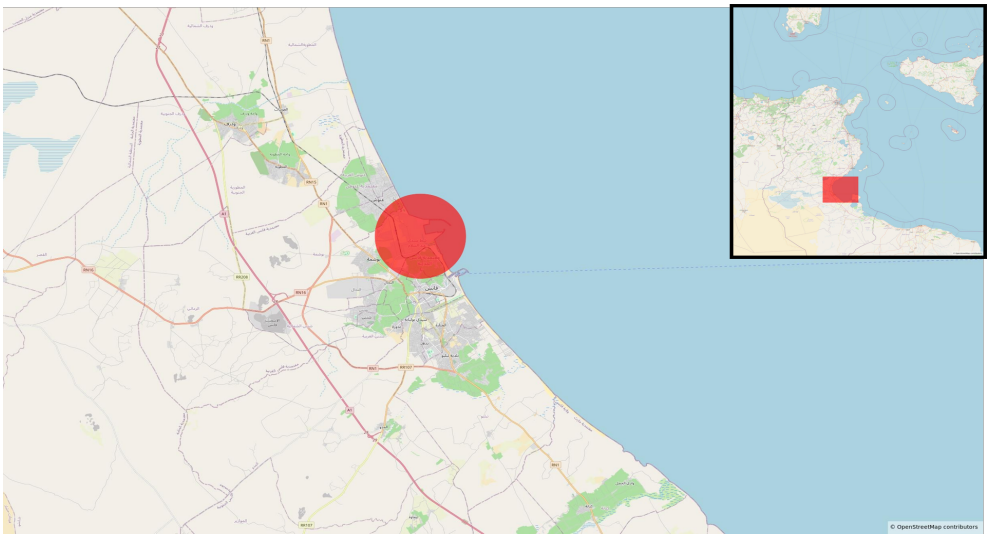

Figure 3.9: Gulf of Gabes: Proposed FPV grid connection site along the coastline. [35]

Tunisia is a global leader in phosphate rock production, with key industrial and chemical complexes in Gabès. These facilities, crucial to the country's economy, transform phosphate ores into various products. To support these energy-intensive operations, developing sustainable energy solutions is essential. One such solution is installing FPV Systems along the coastline of the Gulf of Gabès. Tunisia aims to achieve 30% of its energy production from RESs by 2030, as outlined in the Tunisian Solar Plan. The installation of FPVs will provide a reliable and RESs, efficiently powering the industrial activities in Gabès and contributing to Tunisia's renewable energy goals [41]. The area surrounding the Port of Gabès is ideal for FPVs. This region hosts the Tunisian Chemical Group, established in 1972, specializing in transforming phosphate ores, and other major chemical industries [42]. The strategic placement of FPVs near the Port of Gabès will ensure easy access to high energy demand, providing a consistent and sustainable energy supply to these critical industrial operations. Another advantage, is the higher solar radiation in this region compared to the rest of the country, which is already high across Tunisia [43]: that can reach almost 2300kWh/m2/year.

3.6 Jersey

Jersey is located in the English Channel near the coast of Normandy, France, as it is shown in Fig 3.10. The island covers approximately 118.2 square kilometers and has a population of around 108,000 residents. Jersey enjoys a temperate maritime climate with mild winters and cool summers. The island receives relatively high

levels of sunshine compared to the UK, making it suitable for solar energy projects. The island has significant energy and water needs due to its high population density and economic activities. Given the temperate climate and high sunshine levels, integrating solar energy solutions can help meet these demands sustainably. Jersey's strategic location and favorable climate conditions make it an ideal candidate for renewable energy projects, enhancing its energy security and contributing to environmental sustainability.

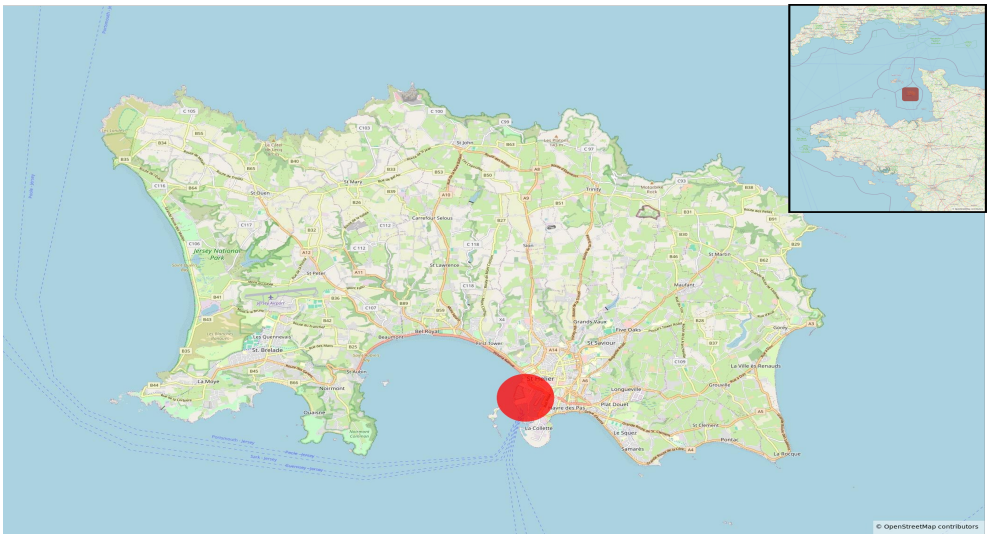

Figure 3.10: Jersey: Proposed FPV grid connection site along the coastline. [35]

Jersey faces several significant energy challenges that necessitate innovative solutions. The island's electricity system, managed by the Jersey Electricity Company, heavily relies on imported electricity from France through an interconnector with a capacity of 120MW [44]. However, this capacity is insufficient to meet Jersey's maximum peak loads, which can reach up to 150MW during the coldest winter evenings. To bridge this gap, Jersey relies on local diesel generators, which are costly to operate and produce high carbon emissions. Additionally, the island faces high costs for imported electricity during peak times, further increasing the economic challenges. Moreover, Jersey has limited land space for expanding RESs like rooftop PV, and there is minimal development in renewable energy infrastructure. A promising solution to these problems is the installation of FPV Systems, which can exploit the island's offshore potential, providing a significant RES without occupying valuable land space. This approach can reduce Jersey's dependence on costly and high-emission diesel generation by supplying clean energy to cover peak loads. Furthermore, FPVs can help mitigate the high costs associated with super-peak pricing by generating electricity locally during peak demand times. By integrating FPVs, Jersey can exploit its surrounding waters to generate renewable

energy, addressing both its energy security and environmental sustainability goals [44]. The main industry facilities are located in the south of the island, in the city of Saint Helier. So, it would be a good spot to connect the system.

3.7 Gotland

Gotland is Sweden's largest island, located in the Baltic Sea approximately 90 kilometers east of the Swedish mainland and 130 kilometers from the Baltic States. It covers an area of about 3,140 square kilometers and has a population of approximately 60,000 residents, with about 23,000 living in Visby. Despite Sweden's general reputation for limited solar potential, Gotland enjoys significantly higher solar irradiance compared to the rest of the country, making it a prime candidate for solar energy projects. The global solar radiation in Sweden is less than 950 kWh/m², while for Gotland it is around 1150 kWh/m² [45]. The island's geographic position in the Baltic Sea and its relatively clear skies contribute to this higher level of sunlight exposure. This can also be seen by the map shown in Fig. 3.11, generated with SOLARGIS [46].

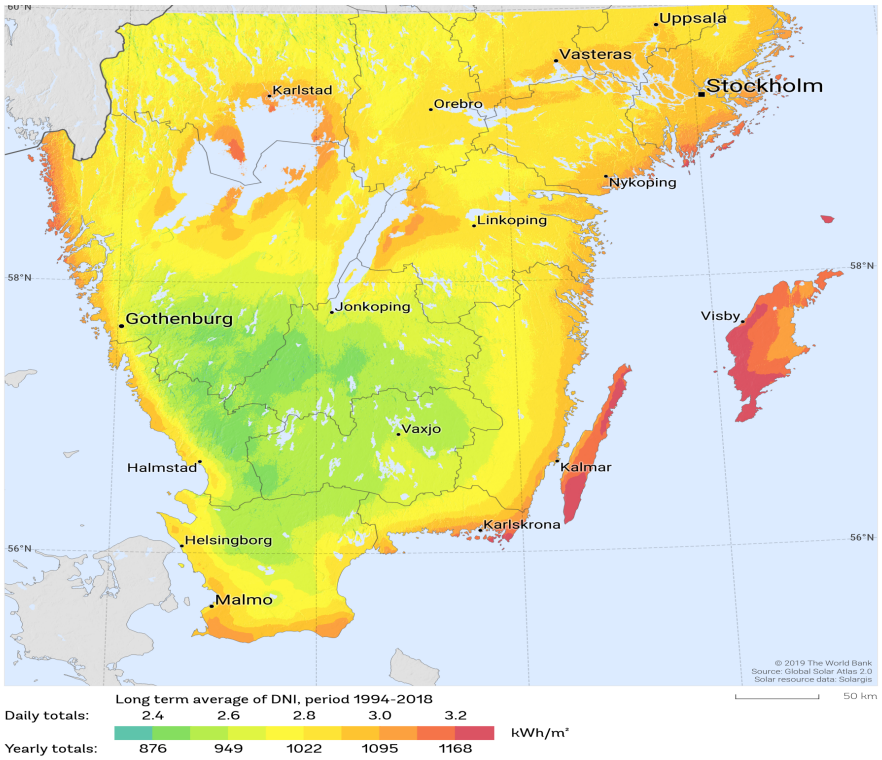

Figure 3.11: Southern of Sweden: Direct Normal Irradiation [46]

In Sweden, ensuring a reliable source of freshwater poses no challenge, but Gotland experiences significant water demand, especially during the summer due to tourism, which saw 950,000 visitors in 2018. In 2015, the total water need was 20.8 million cubic meters, with 3.8 million used by households. Due to summer water shortages, restrictions like banning garden watering have been implemented, and two DSs have been built: Herrvik DP in 2016 and Kvarnåkershamn DP in 2019. Gotland's electricity demand is generally met throughout the year, with an annual usage of about 1,000 GWh and a power need of 120-130 MW, peaking at 180 MW in winter. However, power outages have occurred, prompting projects like Smart Grid Gotland to modernize the grid and increase RES. Gotland aims to utilize 100% RES, including significant wind and solar power installations. The island's grid is connected to Sweden's main grid via an HVDC link with a capacity of 195 MW [47]. By focusing on the DSs, we have that the one in Kvarnåkershamn produces 7500m2/day of clean water versus the 480m2/day of the one in Herrvik. Considering Gotland's significant water needs and its goal of achieving 100% RES , installing a FPVs in front of the DS is a viable solution.

Chapter 4

Data-Driven Platform Classification Based on Reference Site Analysis

To accurately select the best FPV platform design for each chosen marine location, a data-driven approach (DDA) is employed. This approach relies on detailed comparisons of significant wave height (H_s) between reference locations—where FPV systems have already been successfully deployed—and the targeted installation sites. By analyzing and correlating this data, it is possible to objectively determine which FPV system classes offer the best structural compatibility and operational performance for each specific location. By applying this method, real performance data are analyzed, and no models or simulations are needed, making the decisional tool more accurate, and also simplifying the decision-making, since no need for structural analyses or on-site tests, making this operation faster and cheaper.

4.1 Data collection and sources

Significant wave height (H_s) is used as the main parameter to asses the platform suitability. H_s is defined as the average height of the highest one-third of waves observed during a specific measurement period. It is a standard metric used in ocean engineering and coastal studies to characterize wave conditions and assess their potential impact on marine structures: mathematically defined as:

$$H_{1/3} = \frac{1}{N/3} \sum_{j=1}^{N/3} H_j \tag{4.1}$$

Where j is not the sequence number in the record [48]. To implement the

data-driven approach, comprehensive environmental datasets were gathered from validated meteorological and oceanographic sources: More-EST-Platform and ESOX by Lautec, both rely on ERA5 [31], which merges observations and models for consistent climate and wave data. The collected dataset covers a period of 10 years, providing hourly H_s data for both potential installation sites and established reference locations. However, a notable limitation arises from ERA5's spatial resolution of approximately 0.5° (55 km at the equator), which can introduce uncertainties in accurately capturing local wave height variations, particularly in nearshore or sheltered areas.

4.2 Environmental Assessment of Reference Locations

For each platform, at least two locations are needed to have statistical sense data. For Class 1 have been identified three sites of installation have been identified, two from the company Swimsol and a third one, a prototype installed by Hongik University. While the Class 2 sites, one from Ciel&Terre and the other from Sumitomo Mitsui, and for Class 3, two prototypes have been found, one built by SolarSea and the other by Oceans of Energy.

Table 4.1: Reference Floating PV Installations and Their Characteristics.

FPV Type	**Installed Capacity (P_n)**	**Location**	**Coordinates**	**Developer**
Class 1	891 kWp	South Male Atoll, Maldives	4.106166, 73.525695	Swimsol
Class 1	427 kWp	Bawah Reserve, Indonesia	2.514473, 106.040949	Swimsol
Class 1	3.68 kW	Buksin Bay, Korea	34.863095, 128.417212	Hongik University
Class 2	88,038 kWp	Changhua, Taiwan	24.108560, 120.420267	Ciel & Terre
Class 2	80 kWp	Island of Nurai, UAE	24.616598, 54.476092	Sumitomo Mitsui
Class 3	3.25 kW	Baa Atoll, Maldives	5.056940, 73.202271	SolarSea
Class 3	17 kW	Dutch North Sea	52.330337, 4.043162	Oceans of Energy

It's important to observe how this study excludes the superficial platform category, as no large-scale installations of this type currently exist, and available systems are limited to prototype stages [14]. Moreover, their partially submerged configuration introduces substantial uncertainty in energy production estimates due to light attenuation in water. Factors such as water turbidity, biological growth, suspended particles, water clarity, and temperature—which vary significantly by location and over time—make it extremely difficult to accurately analyze their energy efficiency. Accordingly, the focus of this study is on offshore FPV systems utilizing pontoon-type platforms, specifically those categorized as Class 1, Class 2, and Class 3.

Table 4.2 provides key statistical metrics of H_s for each reference location, enabling a better understanding of their environmental profiles:

Table 4.2: Summary of H_s Statistics at Reference Locations.

Location	N	μ_{H_s} **[m]**	$\tilde{H}_s$ **[m]**	σ_{H_s} **[m]**	$H_{s,\min}$ **[m]**	$H_{s,\max}$ **[m]**
South Male Atoll, Maldives	87600	0.73	0.72	0.15	0.40	1.20
Bawah Reserve, Indonesia	87550	0.69	0.68	0.16	0.35	1.15
Buksin Bay, Korea	87590	0.85	0.84	0.18	0.45	1.30
Changhua, Taiwan	87610	1.12	1.10	0.22	0.55	1.70
Island of Nurai, UAE	87580	0.58	0.57	0.14	0.30	1.00
Baa Atoll, Maldives	87570	0.74	0.73	0.15	0.42	1.22
Dutch North Sea	87620	1.35	1.33	0.25	0.60	1.90

The collected H_s data for reference locations generally align well with the expected wave conditions and the type of floating platforms installed. This coherence confirms that the benchmarking method—based on hourly wave height data over 10 years—is reliable in most cases.

However, the data for Changhua, Taiwan, revealed unusually high H_s values that appear inconsistent with the known operational conditions of the platform installed at that site. The location is nearshore and protected by artificial breakwaters (man-made sea walls), which significantly reduce the wave energy reaching the installation area.

To correct this overestimation, a transmission coefficient $\mathrm{K_t}$ is applied. This

factor adjusts the significant wave height to account for the energy dissipation caused by the breakwaters and is defined as:

$$H_{s,\ \text{inside}} = K_t \cdot H_{s,\ \text{offshore}}$$

where $0 < K_{\text{t}} < 1$, representing the fraction of wave energy transmitted past the breakwater. Applying this correction improves the accuracy of the dataset, making it more representative of the real conditions at the Changhua installation site.

To better visualize the wave climate characteristics of each reference location, a box plot analysis was conducted on the significant wave height (H_s) data. To ensure clarity and avoid distortion caused by extreme values, only data below the $x_{99.5}$ were retained, effectively removing statistical outliers from the datasets. This thresholding process can be expressed as:

$$H_s^{\text{filtered}} = \{H_s \mid H_s < x_{99.5}(H_s)\}$$

This approach allows for a more accurate comparison of the wave height distributions across locations. Furthermore, the locations are grouped and color-coded according to their FPV platform classification, providing a clear visual association between wave conditions and platform types, as it is shown in 4.1.

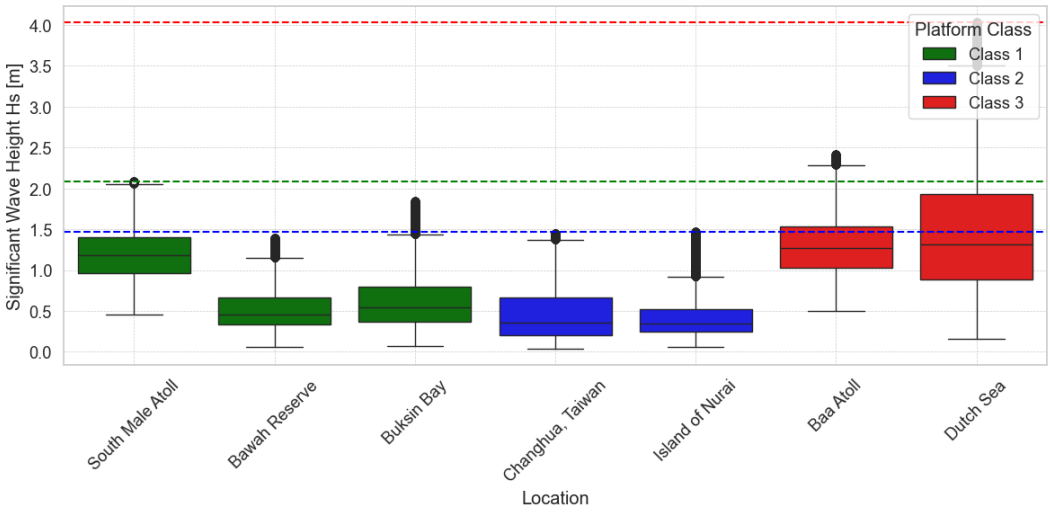

Figure 4.1: Comparison of H_s distributions across reference locations. Values above the $x_{99.5}$ were excluded to remove outliers. Colors correspond to FPV platform classes.

Based on the filtered H_s data and comparison with reference locations, threshold values were defined to categorize the environmental limits each of the three platform types can withstand, as shown in Table 4.3.

Table 4.3: Classification thresholds based on H_s.

Platform Class	Significant Wave Height (H_s)
Class 2	$H_s < 1.47$ m
Class 1	$1.47 \leq H_s < 2.08$ m
Class 3	$2.08 \leq H_s \leq 4.03$ m

These thresholds serve as the basis for classifying potential sites and reflect typical operational limits for existing floating photovoltaic platforms in varying sea states.

4.3 Environmental Assessment of Target Locations

This section provides a detailed environmental classification of the six target locations selected for this study. Following the same methodology used for reference locations, hourly H_s data were extracted and summarized over the full dataset. Table 4.4 presents the key descriptive statistics for each site.

Table 4.4: Summary of significant H_s statistics for target locations.

Location	N	μ_{H_s} [m]	$\tilde{H}_s$ [m]	σ_{H_s} [m]	$H_{s,\min}$ [m]	$H_{s,\max}$ [m]
Ceuta	87,647	0.88	0.77	0.44	0.17	3.96
Gotland	87,647	0.97	0.81	0.66	0.05	6.06
Gulf Gabes	87,647	0.55	0.48	0.30	0.07	3.55
Jersey	87,647	0.83	0.72	0.47	0.12	3.45
Pantelleria	87,647	1.09	0.87	0.78	0.09	6.07
Zadar	87,647	0.47	0.34	0.38	0.04	3.54

As done for the reference locations, a boxplot analysis was also conducted for the target sites to support a clearer interpretation of the wave data. In this case, the H_s values were filtered to exclude the top 0.5% of the data (only values below the $x_{99.5}$ were retained), effectively removing extreme outliers and ensuring a more robust statistical comparison across locations.

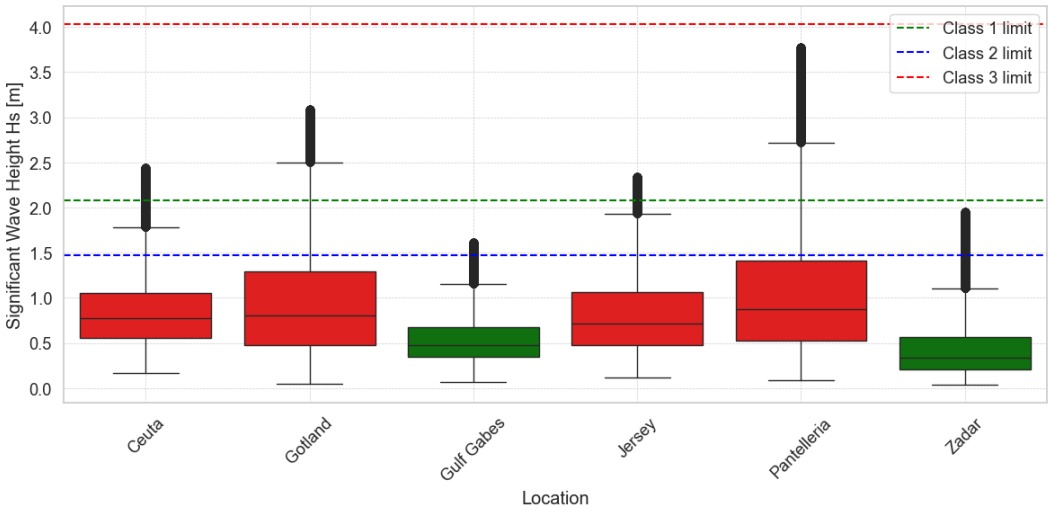

Figure 4.2: Distribution of H_s across the analyzed target locations. Values above the $x_{99.5}$ were excluded to remove outliers. Horizontal dashed lines indicate the class boundaries identified in the reference location analysis.

4.4 Seasonal Removal Decision

The possibility of SR of FPV platforms will be considered for each installation location, to address months characterized by the worst wave conditions. Extreme events can significantly influence the structural design, potentially leading to an unnecessarily robust and expensive platform, for rare events that cover limited periods of the year. To avoid such over-dimensioning, the classification will be refined by excluding the month exhibiting the most extreme wave heights from the design criteria. This approach ensures that the platform selection reflects realistic operational conditions, rather than rare scenarios, enabling the use of lighter and more cost-effective platform types. This will have the consequence of less energy production, since the system will not be operating for a while, and this will be considered during the energy production evaluation. As shown in Fig. 4.3, Ceuta, Gotland, Jersey, and Pantelleria all fall within the threshold of Class 3, while the Gulf of Gabes and Zadar are within Class 1. SR will be considered for Ceuta and Jersey to potentially bring them into Class 1, and for the Gulf of Gabes and Zadar, to move them to Class 2. On the other hand, Pantelleria and Gotland are significantly above the threshold for Class 1 and will not undergo SR, as the reduction in wave height would not be sufficient to change their classification. To determine the appropriate period for SR, an analysis of the monthly variation in H_s was conducted. The approach involves identifying the consecutive months with the highest average H_s values and designating these as non-operational periods.

This strategy helps avoid over-dimensioning the FPV platform for extreme but short-lived conditions. Fig. 4.3 illustrates the average monthly H_s for all target locations. The shaded grey areas highlight the months during which SR is applied.

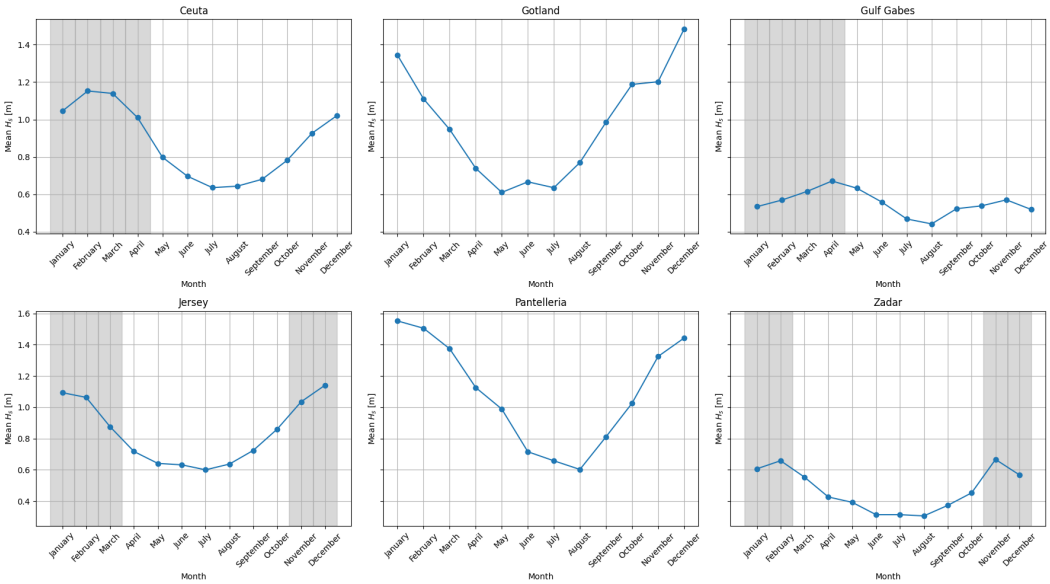

Figure 4.3: Monthly average H_s across the analyzed target locations. The shaded areas indicate the months during which FPV platforms are removed.

Fig. 4.4 shows the modified wave height distributions after SR has been applied. The impact is particularly evident in Ceuta and Jersey, where the exclusion of the most turbulent months successfully reclassifies them from Class 3 to Class 1. Likewise, the Gulf of Gabes and Zadar—initially in Class 1—are upgraded to Class 2. These shifts confirm the effectiveness of seasonal adaptation in reducing design constraints without compromising safety. While this approach does result in some downtime and therefore reduced annual energy output, this trade-off is justified by the substantial benefits in structural optimization and cost reduction. The energy production analysis will later account for these seasonal interruptions to assess the overall feasibility and performance of each installation.

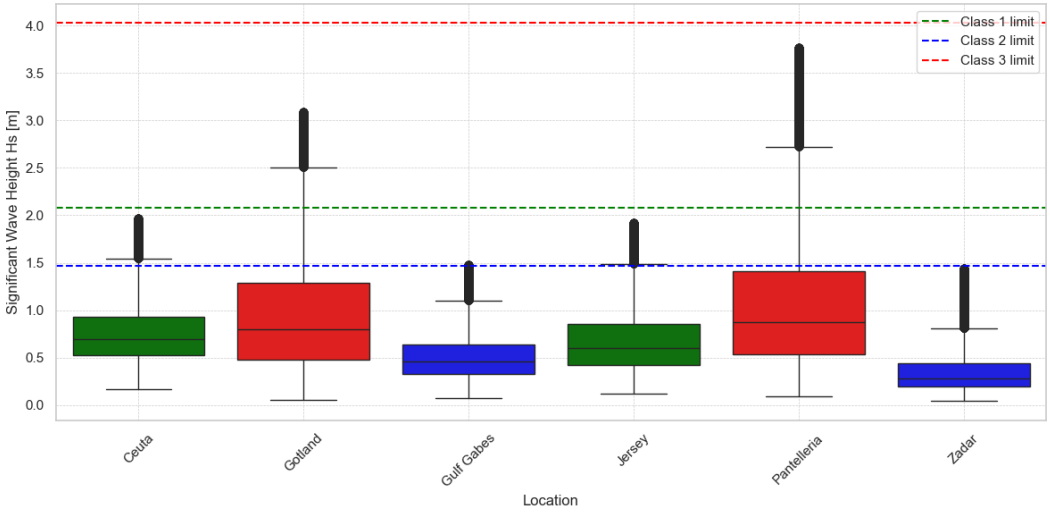

Figure 4.4: H_s distributions for target locations after applying SR. The SR strategy reduces design constraints by excluding the months with the highest wave activity, allowing a reclassification of some sites into lower wave intensity classes.

Chapter 5

Energy Production Analysis

5.1 Solar Irradiance Assessment

To evaluate the energy production of the FPV systems at the selected locations, a first analysis of solar irradiance was carried out. Solar irradiance is a fundamental parameter that directly influences the performance and energy yield of PV systems, and its spatial and temporal variability must be carefully considered in the system design phase.

For this analysis, data were obtained from the Photovoltaic Geographical Information System (PVGIS) [49], a widely used tool developed by the European Commission's Joint Research Centre. PVGIS provides high-resolution historical solar irradiance data derived from satellite observations and ground-based measurements.

Specifically, the hourly irradiance data for 10 years for each of the target locations is extracted. This rich temporal dataset allows for a comprehensive assessment of the solar resource availability, allowing the identification of seasonal patterns and periods of low irradiance that could affect system performance. These irradiance profiles form the basis for subsequent modeling of the expected energy output from the FPV systems.

In order to better visualize the temporal distribution of solar availability, the hourly irradiance data from the past 10 years were first averaged by computing the mean value for each specific hour of each calendar day. This process results in a typical hourly irradiance profile that smooths out year-to-year variability. The averaged hourly values were then summed over each 24 hours to obtain the total daily irradiance, producing a representative time series for a typical year that highlights seasonal patterns and daily fluctuations.

Let $G_{y,d,h}$ represent the irradiance value (in W/m^2) for year y, day d, and hour h. The average hourly irradiance for a typical year is computed as:

$$\bar{G}_{d,h} = \frac{1}{N} \sum_{y=1}^{N} G_{y,d,h} \tag{5.1}$$

where:

- $\bar{G}_{d,h}$ is the mean irradiance for hour h on day d,
- N is the number of years of data (in this case, 10),
- $G_{y,d,h}$ is the irradiance value at hour h on day d in year y.

Then, the daily total irradiance for a representative year is calculated by summing the averaged hourly values for each day:

$$G_d^{\text{daily}} = \sum_{h=1}^{24} \bar{G}_{d,h} \tag{5.2}$$

where G^{daily}_{d} is the total daily irradiance for day d.

The resulting plot, shown in Fig. 5.1illustrates the variation in daily solar energy received at the surface throughout the year for each location. This visualization provides insight into the overall solar potential, highlighting periods of high solar availability as well as low-irradiance seasons, which are critical when estimating the energy yield of the FPV systems.

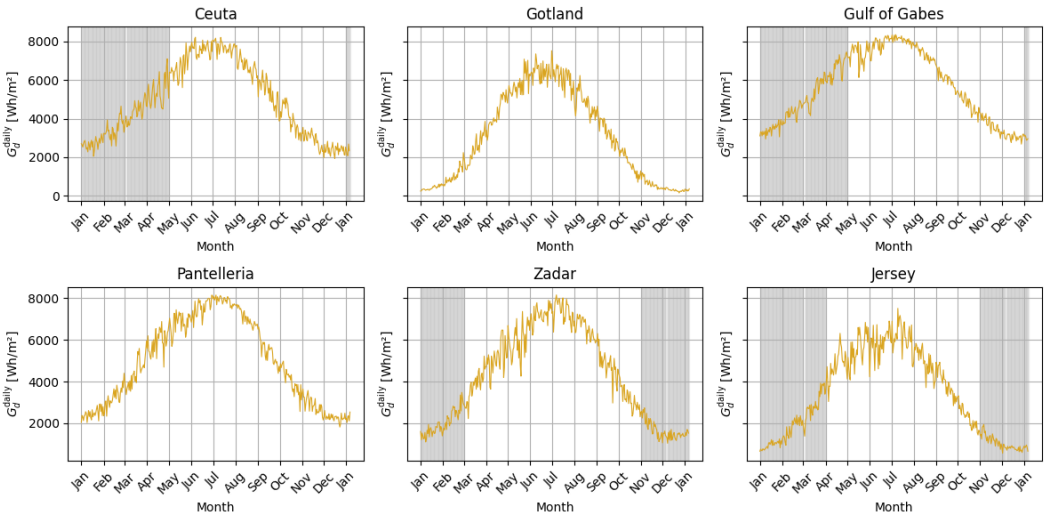

Figure 5.1: Daily average solar irradiance G^{daily}_{d} over the year for each location, where shaded areas indicate the periods during which the FPV systems are removed.

As shown in the Fig. 5.1, all locations exhibit a clear seasonal variation, with lower irradiance levels during the winter months and peaks in summer. Gulf of

Gabes and Pantelleria show the highest overall irradiance, followed by Ceuta and Zadar, while Gotland records the lowest values, particularly in winter. These trends are consistent with expectations based on latitude and reinforce the importance of solar resource availability in selecting suitable sites for offshore FPV systems. Notably, the shaded grey areas representing periods of seasonal FPV removal coincide with the months of lowest solar irradiance. This highlights the strategic value of temporary decommissioning, as it minimizes energy production losses while addressing structural or environmental challenges during less productive seasons.

5.2 PV Module Orientation: Optimal Tilt and Azimuth Settings

This section discusses the setup related to the orientation and the tracking system, and how they change depending on the location and class used. As said in Section 2.2, there are the following assumptions regarding the module angles and setup for each platform class:

- Class 1 platforms are equipped with a fixed optimal tilt angle, optimized for annual yield but not adaptable to changing solar positions throughout the day.
- Class 2 platforms are structurally compatible with single-axis solar tracking systems, enabling them to follow the sun's path and thereby increase energy capture, particularly during early morning and late afternoon hours.
- Class 3 platforms require horizontal mounting of PV modules due to stability constraints. This configuration simplifies installation and improves structural resilience, but results in lower energy yield compared to tilted or tracked systems.

For the locations where the Class 2 platforms are selected, which include a tracking mechanism, it is considered that 1% of the energy produced is used to power the tracking system itself, in line with findings from other techno-economic studies. In this case, the tracking system should be able to evaluate the solar elevation, that is given by the following equation:

$$\theta_s = \arcsin\left(\sin\phi \cdot \sin\delta + \cos\phi \cdot \cos\delta \cdot \cos\omega\right) \tag{5.3}$$

where:

- θ_s: solar elevation angle [°]
- ϕ: latitude of the location [°]

- δ: solar declination angle [°]
- ω: hour angle [°], with $\omega = 0°$ at solar noon and changing by $\pm 15°$ per hour

since its dependence on ϕ is not the same for all locations.

The ideal tilt tracking angle $\beta(t)$ for a single-axis vertical or inclined tracking system is typically adjusted such that the module is perpendicular to the sun's rays:

$$\beta(t) = 90° - \theta_s(t) \tag{5.4}$$

So:

$$\beta(t) = 90° - \arcsin\left(\sin\phi \cdot \sin\delta + \cos\phi \cdot \cos\delta \cdot \cos\omega\right) \tag{5.5}$$

Where t is the time of day, and $\beta(t)$ the optimal tilt angle of the module at time t.

While for the class 1 locations a fixed optimal tilt angle β_{opt} is chosen to maximize the annual energy yield. A commonly used empirical rule is:

$$\beta_{\text{opt}} = \phi - 10° \tag{5.6}$$

where β_{opt} is the optimal fixed tilt angle.

Alternatively, for a balanced energy production throughout the year, the tilt angle may be approximated simply as:

$$\beta_{\text{opt}} = \phi \tag{5.7}$$

In all target locations analyzed in this study, the azimuth angle of the PV modules was set to 0°, which corresponds to a south-facing orientation in the Northern Hemisphere. This orientation is chosen because it maximizes solar exposure over the course of the day, particularly around solar noon when irradiance is at its peak. Since all selected sites are located in the Northern Hemisphere, a south-facing configuration ensures optimal alignment with the sun's path throughout the year.

In Table 5.1, we have summarised the structural classification, geographic coordinates, tilt angle setup, and azimuth orientation for all target locations.

Table 5.1: PV system orientation and configuration per location

Location	Coordinates (Lat, Lon)	Tilt Angle β	Azimuth α
Gulf of Gabes	33.88°N, 10.10°E	$\phi - 10° = 23.88°$	0°
Pantelleria	36.83°N, 11.95°E	0°	0°
Jersey	49.21°N, -2.13°W	$\beta(t)$, see Eq. (5.5)	0°
Gotland	57.47°N, 18.52°E	0°	0°
Zadar	44.12°N, 15.23°E	$\phi - 10° = 34.12°$	0°
Ceuta	35.89°N, -5.31°W	$\beta(t)$, see Eq. (5.5)	0°

5.3 Energy Production Modeling and Cooling Correction

The energy output of FPV systems varies significantly depending on both the geographical location and the structural class of the platform used, as discussed in the previous Sections 5.1 and 5.2. The energy production data for all target locations were obtained using the PVGIS tool, consistently over 10 years, with hourly resolution. In each case, a system loss factor of 15% was directly applied within PVGIS to account for typical Balance of System inefficiencies.

As done for the irradiance data, to reduce interannual variability and generate a representative production profile suitable for system design and performance assessment, the hourly energy outputs were averaged across the 10 years—following the same methodology applied to irradiance data.

Let $P_{h,y}$ denote the power output at hour h of year y, where $h \in [1, 8760]$ and $y \in [1, 10]$. The average hourly power profile $\overline{P}_h$ is then defined as:

$$\overline{P}_h = \frac{1}{N} \sum_{y=1}^{N} P_{h,y}, \tag{5.8}$$

where $N = 10$ is the number of years included in the dataset.

It is important to note that PVGIS assumes ground-mounted PV conditions and does not account for the cooling effects introduced by floating installations. To compensate for this limitation, an additional correction factor γ of 1.10 was applied to the estimated energy production to reflect the expected performance gains from water-based cooling, as reported in the literature [5].

The correct energy production $P_{corr,h}$ at the hour h is calculated as:

$$P_{\text{corr},h} = \gamma \cdot P_h, \tag{5.9}$$

Fig. 5.2 presents the typical $\overline{P}_h$ profiles for each target location for a year. Each subplot displays the average daily power output (corrected using the floating

cooling factor) based on a 10-year dataset. All profiles are generated assuming a nominal system size of 1 MWp, ensuring consistency in the comparison across different sites.

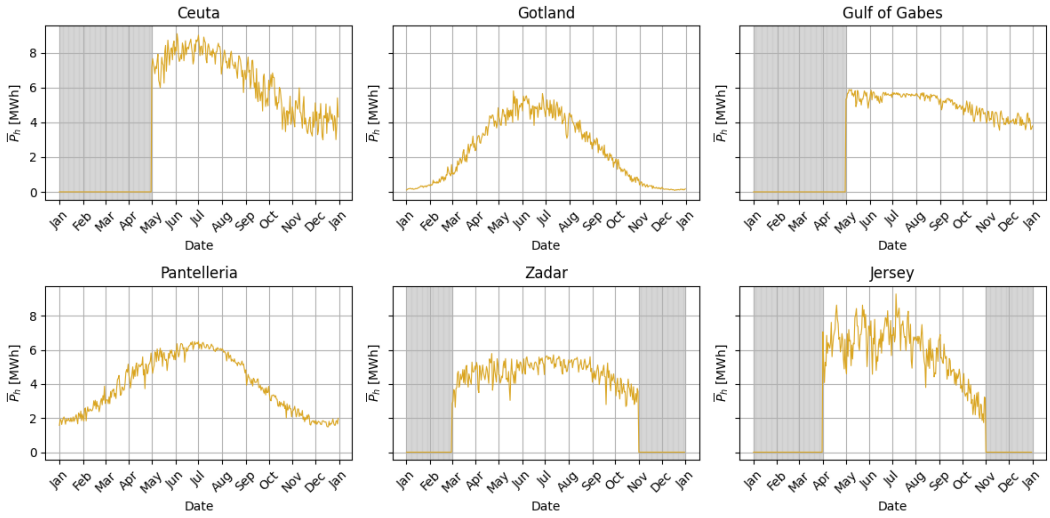

Figure 5.2: Average hourly power $\overline{P}_h$ profiles for all six target locations, taking into account the cooling effects.

To evaluate the long-term energy yield of the FPV system, we estimated the annual energy production over its assumed operational lifetime of 20 years. The first year's production is calculated as the sum of the average daily energy values previously obtained for each location. From the second year onward, a linear performance degradation factor δ of 2% per year is applied, in line with values reported in the literature for floating PV systems.

This means that for year y, where $y \in [2, 20]$, the annual energy output E_y is computed as:

$$E_y = E_1 \cdot (1 - \delta)^{y-1}, \tag{5.10}$$

where E_1 is the total energy produced in the first year. This approach allows for a more realistic estimation of lifetime energy output, taking into account the gradual loss in system performance over time.

In the following Fig. 5.3, the yearly production trend is plotted for each location, showing how energy output declines over time due to the degradation factor. This visual comparison allows for evaluating the expected long-term energy yield at the different locations.

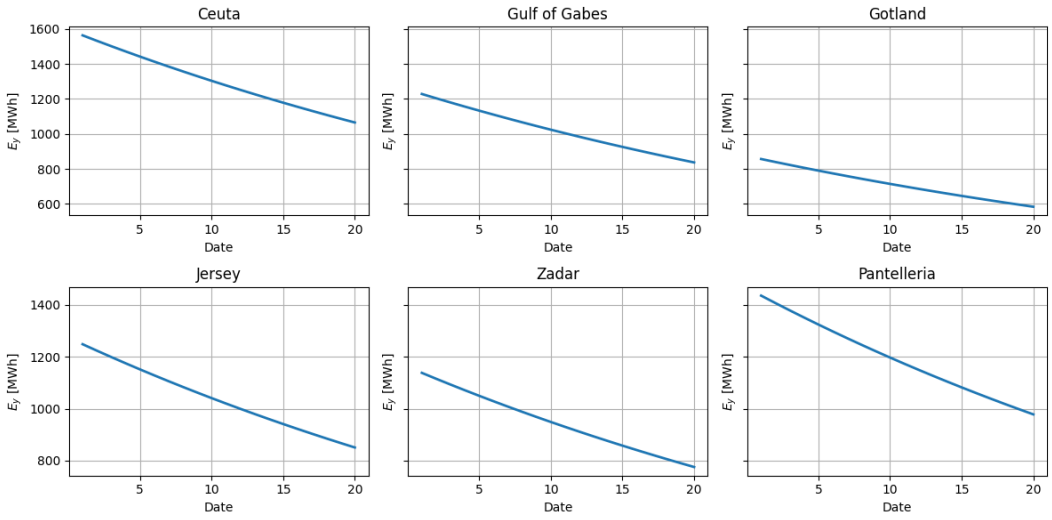

Figure 5.3: Annual energy production E_y for each location over 20 years, accounting for a 2% yearly performance degradation.

Chapter 6

Bottom-up Cost Estimation Methodology

A bottom-up approach (BuA) is employed to evaluate the costs associated with different floating platform configurations and the mooring systems. In this approach, each FPV platform is decomposed into its fundamental structural components, based on specific material properties and geometric characteristics. The cost of each component is estimated individually, and the total platform cost is obtained by aggregating these values [50].

Once the geometry and materials are defined, the total cost of a platform is calculated using the following formula:

$$C_{\text{platform}} = \sum_i (u_i \cdot Q_i) + C_{\text{manufacturing}} \tag{6.1}$$

where u_i represents the unit cost of material i, and Q_i is the corresponding quantity required. The term $C_{\text{manufacturing}}$ accounts for manufacturing and assembly costs, which are estimated based on the complexity of the structure, including factors such as fabrication processes, required labor, and the level of customization.

6.1 Class 1

The material composition and structural configuration of the Class 1 floating platform are based on the design presented by Guido et al. in [9]. As it's shown in Fig.6.1 the platform is divided into three main components: the floaters, the module-supporting frame, and the support structure connecting the frame to the floaters. A platform area of 124 m^2 is considered, allowing for the installation of approximately 70 photovoltaic modules.

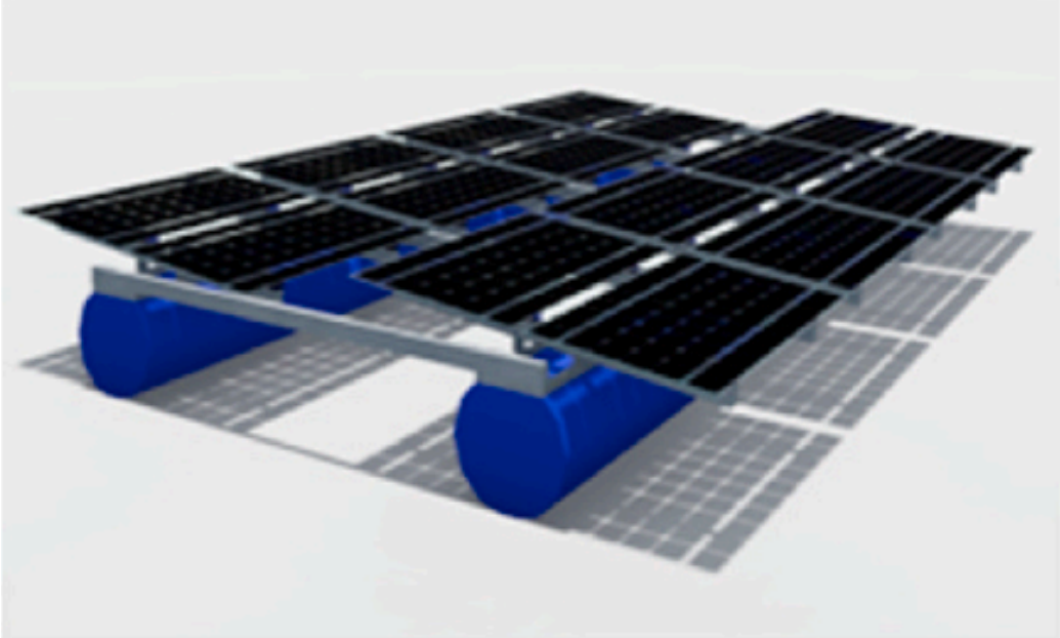

Figure 6.1: Class 1: typical floater design [10].

The materials selected for each component were chosen based on mechanical performance, corrosion resistance, and cost-effectiveness for offshore environments. The Support structure is made of AISI 205 steel, selected for its structural strength and corrosion resistance in saline conditions. While the Frame structure comes from Aluminium 5005, which offers a balance between lightweight and high corrosion resistance, suitable for components under lower structural loads, and the floaters are fabricated from High-Density Polyethylene (HDPE), chosen for its UV and saltwater resistance, mechanical robustness, and relatively low cost.

Table 7.1 summarizes the material usage, cost per kilogram, and total cost associated with the fabrication of one Class 1 platform:

Table 6.1: Cost breakdown of Class 1 materials, including unit price, weight, and total cost.

Material	**Mass**	**Cost**	**Total Cost**
Aluminium 5005	138.1	2.43	336
Steel AISI 205	2,615.1	3	7,845
HDPE	265.36	1.216	1,291
*	kg	€/Kg	€

This structured breakdown enables a detailed and transparent cost estimation,

forming the basis for further techno-economic analysis of Class 1 systems.

In Table 6.2, the overall cost estimation is completed by including the manufacturing and assembly expenses

Table 6.2: Total cost summary for Class 1 platform, including material and manufacturing costs.

Material/Service	Cost	Unit of Measure
Aluminium 5005	336	€
Steel AISI 205	7,845	€
HDPE	1,291	€
Manufacturing work, assembly	1,894	€
Total	**11,366**	€

6.2 Class 2

For the Class 2 system, the design adopted is based on the commercially available Hydrelio platform developed by Ciel & Terre [22]. This modular system consists of floaters capable of supporting individual photovoltaic panels, with a detailed structural layout illustrated in Fig. 6.2.

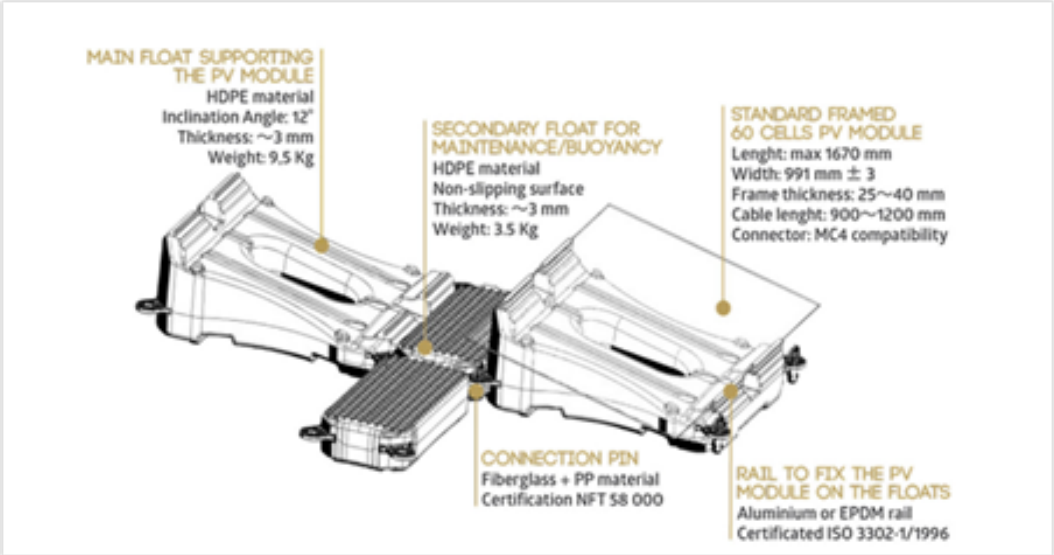

Figure 6.2: Class 2: floater design from Ciel&Terre [22].

Each floater includes a main float and a secondary float, both entirely constructed from HDPE. A mounting rail system made of Aluminium 5005 is used to secure the PV modules. According to Ghigo et al. [9], the aluminium requirement is estimated at 2 kg per module. The material usage and associated costs per floater are summarized in Table 6.3:

Table 6.3: Cost breakdown of Class 2 materials, including unit price, weight, and total cost.

Material	Mass (kg)	Cost (€ /kg)	Total Cost (€)
Aluminium 5005	2	2.43	4.86
HDPE	13	4.86	63.86

Given the more intricate geometry of the Hydrelio system and the modular assembly required, an additional 40% manufacturing and assembly overhead is applied.

Table 6.4 summarizes the cost breakdown for the Class 2 platform, including material costs and the estimated manufacturing and assembly expenses:

Table 6.4: Total cost summary for Class 2 platform, considering materials and increased manufacturing complexity.

Material/Service	Cost	Unit of Measure
Aluminium 5005	4.86	€
HDPE	63.86	€
Manufacturing work, assembly	27.5	€
Total	**96.2**	€

For Class 2, multiple floats are considered to be connected through pins to form a single platform measuring 10x10, consisting of 100 floats and 100 modules. As such, the total cost of one Class 2 platform is 9,620 €.

6.3 Class 3

For the Class 3 system, the platform concept developed by SolarDuck [51], a Dutch company specializing in offshore floating solar technology, is considered. Their full-scale pilot features four interconnected triangular platform units, each supported by floating pillars. The structure is entirely made of aluminium, elevating the

solar panels and electrical components over three meters above the water surface, providing protection from waves. According to Norsk Hydro [52]—the supplier of the aluminium profiles used in the pilot—each triangular side measures approximately 16 meters, forming a stable and modular offshore solar island. Each platform can host 80 modules.

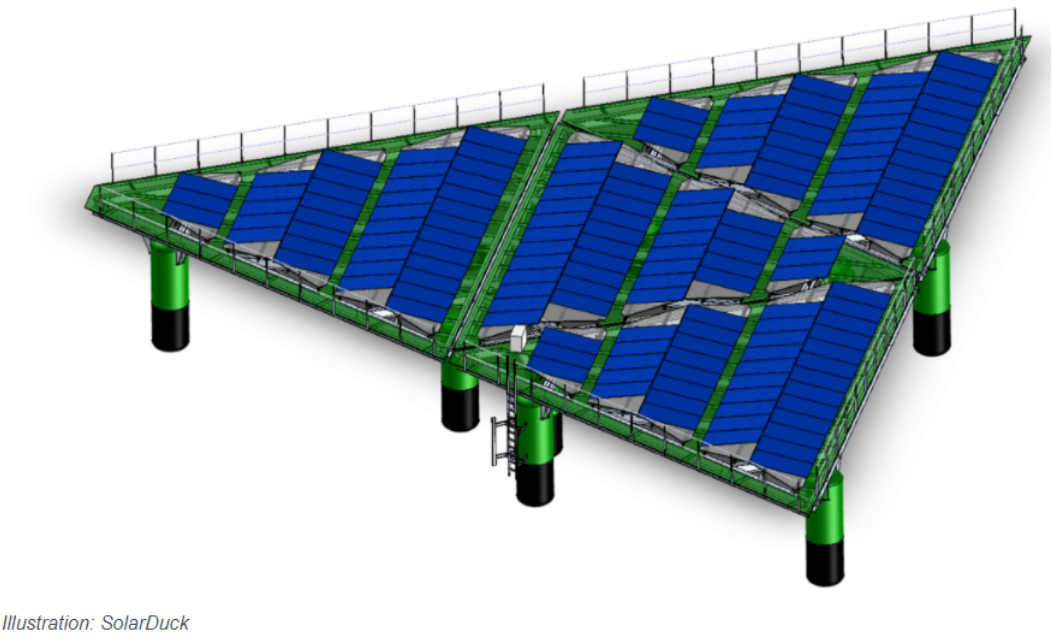

Figure 6.3: Class 3: floater design from SolarDuck [51].

The estimated material usage and associated costs for the Class 3 SolarDuck platform are summarized in Table 6.5. The structure primarily consists of aluminium, supported by HDPE and stainless steel components.

Table 6.5: Cost breakdown of Class 3 materials, including unit price, weight, and total cost.

Material	Mass (kg)	Cost (€/kg)	Total Cost (€)
Aluminium 5005	3,500	2.43	8,505
HDPE	1,500	1.22	1,830
Stainless Steel	500	3	1,500

Due to the more complex structure and larger scale of the Class 3 platform, manufacturing and assembly processes are significantly more demanding. As a result, an additional 40% overhead is assumed to account for the increased difficulty

in fabrication and transport. Table 6.6 presents the cost breakdown for the Class 3 platform, including individual material costs and the estimated expenses for manufacturing and assembly:

Table 6.6: Total cost summary for Class 3 platform, considering materials and increased manufacturing complexity due to the modular Hydrelio design.

Material/Service	Cost	Unit of Measure
Aluminium 5005	8,505	€
HDPE	1,830	€
Stainless Steel	1,500	€
Manufacturing work, assembly	4,668	€
Total	**16,503**	€

6.4 Mooring and anchoring system

The FPV platforms will use a catenary mooring system, anchored securely to the seabed with drag-embedded anchors. This system design provides the necessary flexibility to withstand varying sea conditions, which is essential for offshore floating PV installations. The mooring chain length l_{chain} is determined by the sea depth H_d, with the total length required being 1.4 times the sea depth. This length is longer than the sea depth by 40% to ensure that the chain is not taut; this slack is necessary to allow free movement of the platform. By doing so, the mechanical stresses on the mooring system are reduced [9]. So the chain length can be calculated as follows:

$$l_{chain} = 1.4 \cdot H_d, \tag{6.2}$$

The main properties of the mooring chain are summarised in Table refmaterial-chain.

Table 6.7: Summary of the main characteristics of the mooring chain.

Characteristic	Value	Unit of Measure
Diameter	0.03	m
Unit weight	18.2	kg/m
Cost Steel	2.75	€/kg

Using the available data, the cost of the mooring chain per line is calculated as:

$$C_{\text{chain}} = l_{\text{chain}} \cdot 18.2 \cdot 2.75, \tag{6.3}$$

where 18.2 is the chain mass per meter [kg/m], and 2.75 is the cost per kilogram [€/kg].

For the drag-embedded anchors, the cost depends on the Minimum Breaking Load (MBL) required by the mooring system. In this study, the MBL is estimated to be 736 kN for all platforms, based on structural constraints and safety considerations [9]. The anchor cost is calculated using the following formula:

$$C_{\text{drag}} = MBL \cdot \frac{0.052}{9.81}, \tag{6.4}$$

resulting in:

$$C_{\text{drag}} = 736{,}000 \cdot \frac{0.052}{9.81} \approx 3{,}901.32 \text{ €} \tag{6.5}$$

Therefore, the total cost of a single mooring line is given by:

$$C_{\text{mooring}} = C_{\text{chain}} + C_{\text{drag}}. \tag{6.6}$$

This method offers a robust and detailed approach for estimating the mooring system costs of a generic floating PV platform, accounting for structural flexibility and hydrodynamic motion requirements.

Assuming a fixed distance from shore d_{coast} of 1,000 m and a water depth of 40 m, the chain length per mooring line is set to 56 m. The number of mooring lines required varies by platform class:

- Class 1: 1 mooring line per platform
- Class 2: 1 mooring line per aggregated float structure
- Class 3: 2 mooring lines per platform (due to increased structural loads and complexity)

Substituting the values, the mooring cost per line becomes:

$$C_{\text{mooring}} = 56 \cdot 18.2 \cdot 2.75 + 3{,}901 = 5{,}802 \text{ €/line} \tag{6.7}$$

6.5 Electrical components

As mentioned in Section 2.3, there are two main layout options for the electrical design. The first places all the necessary electrical components—such as inverters and transformers—on the floating platforms. In this case, the electricity is converted

to AC offshore, and an underwater AC cable is used to transmit it to the shore [9]. The alternative approach is to transmit the electricity as DC via a submarine cable and carry out the voltage and frequency conversion at an onshore substation [18]. This study adopts the second option. The costs of the key electrical components are summarized in the Table
refcost-eletrical:

Table 6.8: Estimated costs for electrical infrastructure components.

Component	Cost	Unit of Measure
Submarine DC cable	2.18	k€/(MW·km)
On-shore substation	157.36	k€/MW

For a given P_n and a d_{coast} , it's possible to determine the total cost of the substation $C_{\text{substation}}$ and of the submairne cable C_{cables} :

$$C_{substation} = 157{,}360 \cdot P_n \tag{6.8}$$

$$C_{cables} = 2.18 \cdot P_n \cdot d_{coast} \tag{6.9}$$

For the photovoltaic panel, the SunPower Maxeon 3 model is considered, which has a nominal power of 400W and a cost of 300€ per unit [9]. So the total cost of the PV modules is avaluted strating from the P_n :

$$C_{\text{PV}} = \frac{P_n}{P_{\text{panel}}} \cdot C_{\text{panel}} \tag{6.10}$$

Chapter 7

Energy, Environmental, and Economic Assessment

7.1 Economic Analysis

The economic viability of the project is assessed through the estimation of the Net Present Value NPV, considering various configurations with different numbers of modules to identify the most profitable option. The NPV is an economic indicator used to evaluate the profitability of a cash flow resulting from a specific investment [53]. It is calculated by summing the discounted net cash flows $\mathrm{B_t}$ over the plant's lifetime and subtracting the initial investment cost i , using a nominal discount rate i provided by the investor. Since the technology is new, it means it has a high level of risk; an i of 6.4% is choosen [9]:

$$\mathrm{NPV} = -I + \sum_{t=1}^{n} \frac{B_t - MC_t}{(1+i)^t}, \tag{7.1}$$

The i corresponds to the capital expenditures $CapEx$, which are composed of several components:

$$I = \mathrm{Capex} = C_{\mathrm{con}} + C_{\mathrm{el}} + C_{\mathrm{platform}} + C_{\mathrm{mooring}} + C_{\mathrm{PV}} + C_{\mathrm{installation}}, \tag{7.2}$$

Where $\mathrm{C_{platform}}$ and C_{mooring} are evaluated through the bottom-up approach. For the project to be economically sustainable, a positive NPV must be achieved. This indicator is useful for comparing different investment options and quantifying the actual monetary return. The term $\mathrm{MC_t}$ accounts for the maintenance cost during each period, which represents the operational expenditures $OpEx$, and is defined as:

$$MC_t = \text{OpEx} = 0.025 \cdot \text{CapEx} \tag{7.3}$$

In this analysis, the B_t is derived from the avoided cost of electricity that would otherwise be supplied through a combination of grid and diesel generation sources, as shown in eq. 7.4.

$$B_t = \text{Energy}_t \cdot C_{\text{kwh}} \tag{7.4}$$

Since the selected locations are semi-isolated in several cases, to evaluate the cost of the energy (C_{kWh}), we assume that 80% of the electricity demand is covered by the national grid, while the remaining 20% is generated locally using diesel generators. According to the study by Casillas et al. [54], the fuel consumption of typical 110 kW and 55 kW diesel generators (η_{diesel}) ranges between 0.41 and 0.52 liters per kWh under standard operating conditions. By combining this consumption range with the local diesel prices (C_{diesel}) retrieved for each target location [55] and local household electricity prices (C_{grid}) [56, 57], we estimate the cost per kWh of electricity generated by diesel ($C_{\text{diesel-kWh}}$). The resulting C_{kWh} used in this analysis is the average between the grid price and the diesel-based generation cost. The results are summarized in Table 7.1:

Table 7.1: Cost breakdown of Class 1 materials, including unit price, weight, and total cost.

Location	$\mathbf{C}_{\text{diesel}}$ (€/L)	$\mathbf{C}_{\text{diesel-kWh}}$ (€/kWh)	$\mathbf{C}_{\text{grid}}$ (€/kWh)	$\mathbf{C}_{\text{kWh}}$ (€/kWh)
Ceuta	1.37	0.637	0.115	0.2194
Gotland	1.75	0.814	0.087	0.2324
Gulf of Gabès	0.66	0.307	0.184	0.2086
Jersey	1.65	0.767	0.085	0.1880
Pantelleria	1.60	0.744	0.160	0.2814
Zadar	1.29	0.600	0.117	0.2424

The cost per kilowatt-hour of electricity generated by a diesel generator $C_{\text{diesel-kWh}}$ is estimated using the following equation:

$$C_{\text{diesel-kWh}} = C_{\text{diesel}} \cdot \eta_{\text{diesel}} \tag{7.5}$$

Where the average fuel consumption η_{diesel} used for this calculation is:

$$\eta_{\text{diesel}} = \frac{0.41 + 0.52}{2} = 0.465 \text{ L/kWh} \tag{7.6}$$

The final C_{kWh} used in the analysis is calculated as a weighted average, where 80

$$C_{\text{kWh}} = 0.2 \cdot C_{\text{diesel-kWh}} + 0.8 \cdot C_{\text{grid}} \tag{7.7}$$

In this analysis, parameters such as unit selling price, and retail value are assumed to remain constant throughout the system's lifetime. The NPV does not account for uncertainties related to these variables. Based on these assumptions, it is possible to compute the NPV over time and determine the point at which the investment breaks even. This corresponds to the Payback Time t_{PBT}, which is defined as the period required to recover the initial investment through accumulated savings or revenues [53]. The t_{PBT} is determined by the condition:

$$\text{PBT} = t_{\text{PBT}} \quad \Rightarrow \quad \text{NPV}(t_{\text{PBT}}) = 0 \tag{7.8}$$

The Levelized Cost of Energy (LCOE) is another critical economic metric used to assess the cost-effectiveness of energy generation. It represents the per-unit cost of energy produced by the system, taking into account both $CapEx$ and $OpEx$ over the project's lifetime [7].

$$\text{LCOE} = \frac{I + \sum_{t=1}^{n} \frac{MC_t}{(1+i)^t}}{\sum_{t=1}^{n} \frac{E_t}{(1+i)^t}} \tag{7.9}$$

7.1.1 Installation Cost

Estimating the installation cost of the floating structure and its mooring system presents a challenge due to the emerging nature of the technology and the limited availability of real-world cost data. To address this, the methodology adopted in [18] is applied. This approach is adapted from offshore wind industry practices and accounts for variables such as vessel chartering, installation time, and travel distance from shore. The installation cost is expressed as:

$$C_{\text{Install\_FPV}}(x, y) = n_{\text{FPV}} \left[T_{\text{install}} + \frac{2d(x, y)}{v_{\text{boat}}} \right] \cdot \frac{C_{\text{boat}} + C_{\text{divers}} + C_{\text{workers}}}{n_{\text{FPV\_pertrip}}} \tag{7.10}$$

Where:

1. n_{FPV}: total number of floating units to be installed in the project.
2. $n_{FPV\_pertrip}$: number of floating units that can be transported and deployed per trip by the installation vessel.
3. $T_{install}$: time required to install a single FPV unit once on site.

4. d(x, y): distance from the installation site to shore, expressed as a function of its spatial coordinates.
5. v_{boat}: speed of the jack-up vessel used during the transport and installation phases.
6. C_{boat}: daily or hourly charter cost associated with the use of the jack-up vessel.
7. C_{divers}: cost of divers (per unit of time).
8. $C_{workers}$: cost of workers (per unit of time).

The input parameters used in the equation are summarized in Table 7.2:

Table 7.2: Input parameters used for the installation cost estimation.

Symbol	Value	Unit of Measure	Source
n_{FPV}	Depends on system size	–	Assumed
$n_{FPV\_pertrip}$	Depends on class type	units/trip	-
$T_{install}$	0.5	hours/unit	-
d(x, y)	-	km	-
v_{boat}	2000	m/h	[18]
C_{boat}	120	€/h	[58]
C_{divers}	50	€/h	[58]
$C_{workers}$	90	€/h	[58]

The $T_{install}$ of each platform and $n_{FPV\_pertrip}$ are assumed by taking into account the values of deployment of similar offshore technologies. In the case of Class 1 and Class 2, we consider 5 units transported per trip, while for Class 3 we consider 2 platforms per trip. This model enables a more structured and location-sensitive estimation of installation costs for FPV systems, particularly in the absence of historical installation cost data.

7.1.2 Comparative Plots

To enable a fair comparison across all selected locations, we fix key parameters: a H_d of 40 m, d_{coast} equal to 1,000 m, and a P_n of 1 MWp.

Based on these standardized conditions, the following plot illustrates the cost breakdown of the FPV for each location. As anticipated, the costs related to panels

and electrical components remain consistent across different locations, as they are independent of the system class. In contrast, the mooring, platform, and labor costs vary significantly depending on the class of the system, with Class 3 installations being noticeably more expensive than Class 1 and Class 2.

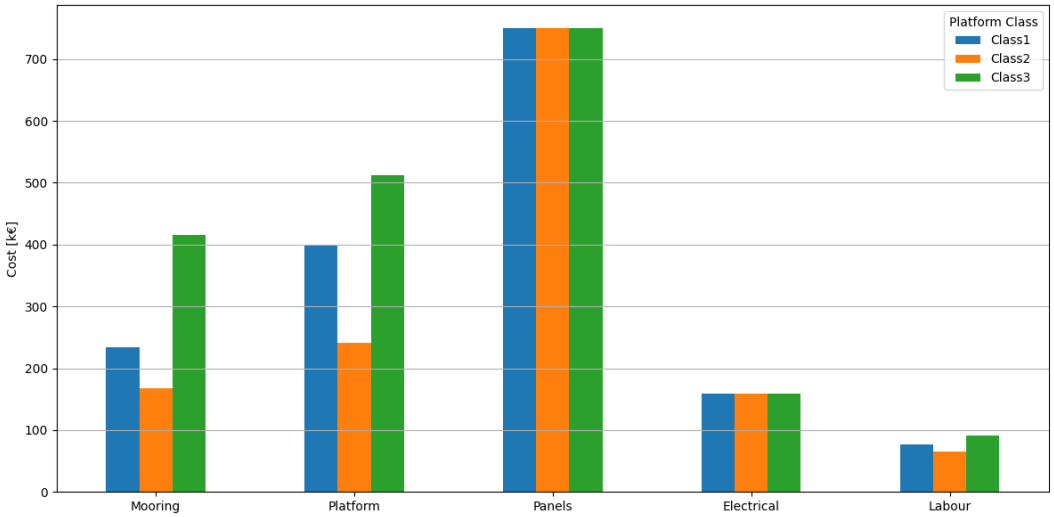

Figure 7.1: Cost breakdown by component for each system class at H_d=40 m depth, d_{coast}=1,000 m , and P_n=1MWp

Additionally, the pie charts in Fig. 7.2 illustrate the relative share of each cost component for the different system classes. Notably, the share of platform costs is highest for Class 3 systems, reaching approximately 27%, while for Class 2 it accounts for only around 17%. This visual representation highlights how the choice of system class significantly influences the distribution of total costs.

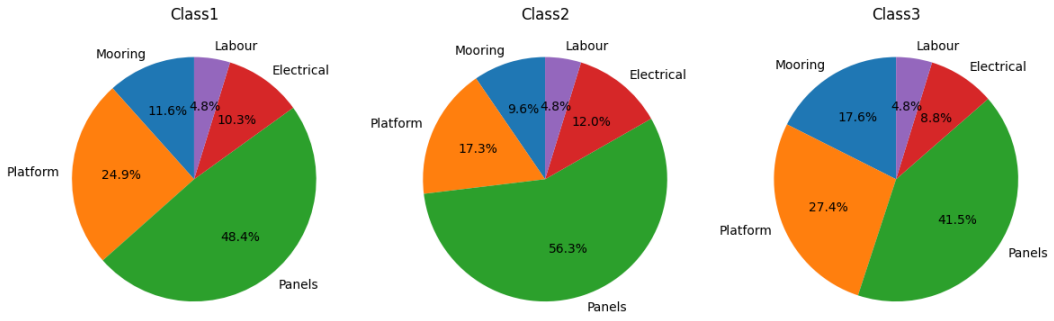

Figure 7.2: Share of cost components for each class.

The following plot presents the results of a sensitivity analysis on *CapEx*,

conducted by varying the P_n from 0.1MW to 2MW in increments of 0.1MW. The analysis reveals a linear increase in capital costs for all classes. However, as the nominal power increases, the cost trajectories begin to diverge, with the gap between the system classes widening. This indicates that higher capacity systems amplify the cost differences between Class 1, Class 2, and Class 3 configurations.

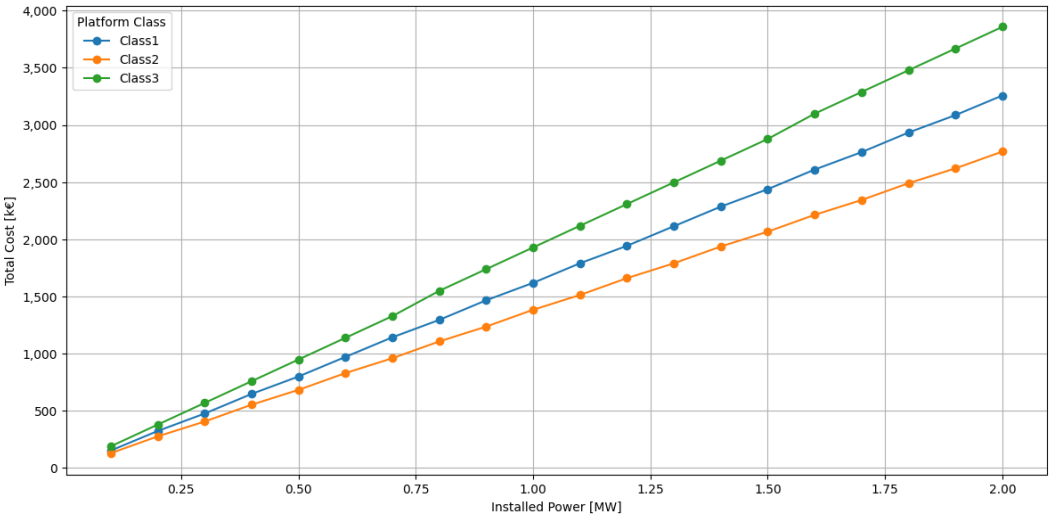

Figure 7.3: *CapEx* sensitivity to P_n.

Table 7.3 presents the *CapEx* and *OpEx* values for each location. The *OpEx* are broken down into fixed cost (e.g., maintenance, monitoring) and additional SR cost, which applies only to Class 1 and Class 2 systems. As a result, these classes exhibit significantly higher total *OpEx* compared to Class 3 systems, which do not require seasonal disassembly and redeployment. This highlights how structural class influences not only the *CapEx* but also long-term *OpEx*, with Class 3 sites being more cost-efficient in terms of annual *OpEx*.

Table 7.3: *OpEx* and *CapEx* estimates for different locations and platform classes, evaluated at H_d=40 m depth, d_{coast}=1,000 m , and P_n=1MWp

Location	**Platform Class**	**Seasonal Removal** *OpEx* **[k€/y]**	**Fixed** *OpEx* **[k€/y]**	**Total** *OpEx* **[k€/y]**	*CapEx* **[k€]**
Ceuta	Class1	13.23	15.00	28.23	1,619.09
Gotland	Class3	0.00	15.00	15.00	1,928.63
Gulf of Gabes	Class2	9.45	15.00	24.45	1,383.53
Pantelleria	Class3	0.00	15.00	15.00	1,928.63
Zadar	Class2	9.45	15.00	24.45	1,383.53
Jersey	Class1	13.23	15.00	28.23	1,619.09

Figure 7.4 illustrates the NPV evolution over the 20-year project lifetime for all locations. The analysis shows that the project is economically feasible in almost all locations, where the NPV becomes positive before the end of the project horizon. This indicates that the initial investment and operational costs are outweighed by the revenues generated from energy production. In contrast, the only location that does not reach a positive NPV within 20 years is Gotland, suggesting that under the current assumptions, the project would not be financially viable in these cases.

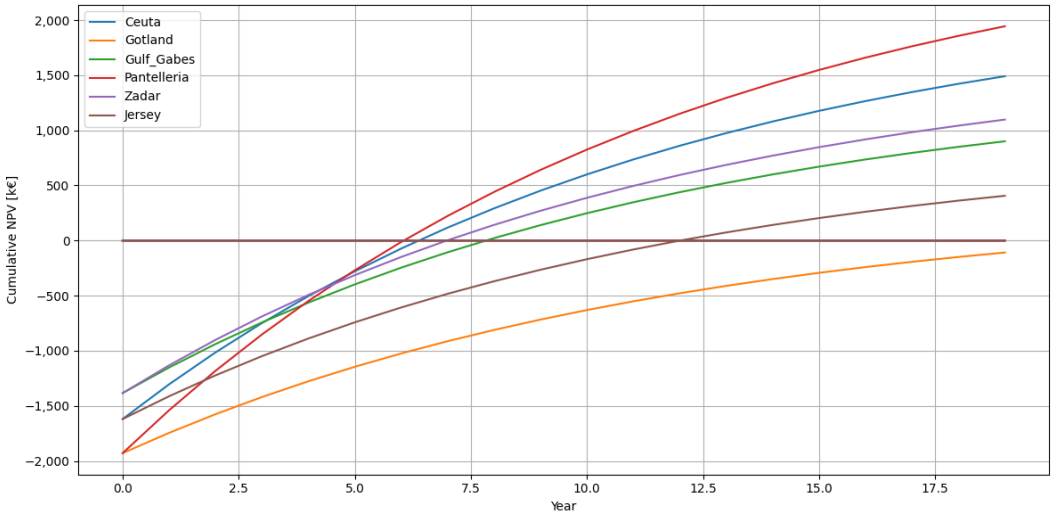

Figure 7.4: NPV over 20 years for each location.

7.2 CO2 Emissions Avoided

One of the primary environmental benefits of deploying FPV systems is the reduction in carbon dioxide (tCO_2) emissions through the displacement of fossil fuel-based electricity generation. This section quantifies the total tCO_2 emissions avoided at each selected location by substituting a portion of the local energy demand with electricity produced by the FPV systems.

To estimate the emissions avoided, the analysis assumes that the electricity generated by the FPV system offsets the average local electricity mix, which, in many semi-isolated or island regions, includes a significant share of diesel-based generation. The emissions avoided are calculated using the following expression:

$$\mathrm{CO}_{2,\mathrm{avoided}} = E_y \cdot EF_{\mathrm{avg}} \tag{7.11}$$

Where EF_{avg} is the average emission factor of the displaced electricity source, expressed in tons of CO_2 per megawatt-hour ($kgCO_2/MWh$).

The EF_{avg} used in this analysis are based on a combination of data sources: for electricity from the national grid were retrieved from the public dataset provided by Our World in Data [59], which reports the carbon intensity of electricity generation across countries. For diesel-based generation, the average emission factor was taken from the study by Jakhrani et al. [60], which assessed the carbon footprint of various diesel generators with different rated powers. According to their findings, the average EF_{avg} from diesel-based electricity production is estimated at 1.585 $kgCO_2/kWh$. A weighted average EF_{avg} for each location is then calculated based on the assumed energy mix—20% from diesel and 80% from grid electricity—to reflect the hybrid nature of power supply in semi-isolated regions, as done for the energy price in the 7.1.2.

$$EF_{\mathrm{avg}} = 0.2 \cdot EF_{\mathrm{diesel}} + 0.8 \cdot EF_{\mathrm{grid}} \tag{7.12}$$

In the Table 7.4 are summarised, the results related to the average emission factor for each location EF_{avg}, where E_t the first year is considered.

Table 7.4: Estimated annual tCO_2 emissions avoided by FPV deployment at each location.

Location	**E_t (MWh)**	**Grid EF (tCO_2/MWh)**	**EF (tCO_2/kWh)**	**tCO_2 (t/year)**
Ceuta	1563.74	0.115	0.4090	639.57
Gotland	856.49	0.036	0.3458	269.17
Gulf of Gabès	1228.40	0.560	0.7650	939.72
Pantelleria	1435.89	0.288	0.5474	786.01
Zadar	1138.26	0.174	0.4562	519.27
Jersey	1248.67	0.044	0.3522	439.78

As shown, the amount of avoided emissions varies not only with the energy yield of the FPV system but also with the local carbon intensity of the existing electricity supply. Locations with a higher reliance on diesel generation, such as Pantelleria and the Gulf of Gabès, exhibit greater emission reduction potential. On the other hand, regions with cleaner electricity mixes, such as Gotland, still benefit from FPV deployment but to a lesser extent in terms of tCO_2 avoided.

Figure 7.5 shows the cumulative tonnes of CO_2 avoided over the system's lifetime for each location.

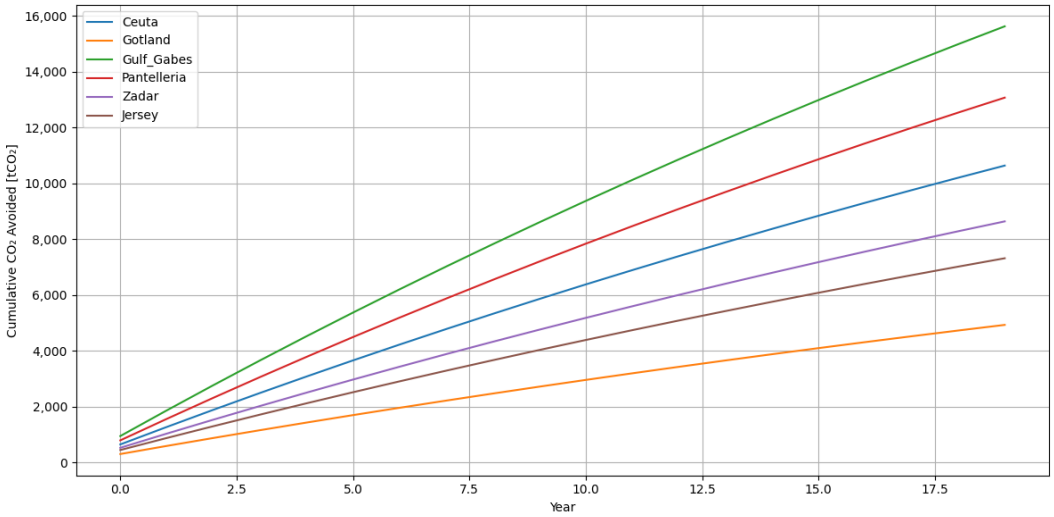

Figure 7.5: Cumulative tCO_2 emissions avoided over time for each location.

These findings underline the dual benefit of FPV systems in such contexts: providing renewable electricity while contributing to climate change mitigation through substantial emission reductions.

Chapter 8

Results and Discussion

8.1 Analysis and Interpretation of the Data-Driven Results

One of the main findings of this study is the successful application of DDA to classify offshore FPV platform types based on H_s. Instead of relying on theoretical modeling or site-specific structural analysis, this approach uses historical wave data from existing FPV installations to define operational thresholds for three platform classes. By analyzing 10 years of hourly H_s data and filtering out extreme outliers (above the 99.5th percentile), clear classification limits were established. These were then used to assess the six target locations, enabling the selection of appropriate platform types in a fast, consistent, and resource-efficient manner, where the results are summarised in the table 4.3. This represents a key novelty of the study, as no prior work has proposed any classification system for offshore FPV platforms based on environmental conditions, making this the first attempt to define quantitative thresholds linked to platform typologies. However, one of the limitations of the proposed method lies in the use of ERA5 data, whose spatial resolution of approximately 0.5° (about 55 km at the equator) may introduce uncertainties in accurately capturing local wave height variations—especially in nearshore or sheltered areas. Another important limitation is that the classification is based solely on H_s, without considering other relevant environmental loads such as wind, currents, or the wave period. The absence of these parameters may lead to an oversimplified structural assessment, which could limit the applicability of the method in more complex offshore scenarios. However, the results obtained for the assigned platform types across the six target locations align well with initial expectations based on their known sea conditions, supporting the reliability and practical relevance of the proposed classification method.

8.2 Conclusions on the Energy, Environmental, and Economic Impacts

The BuA employed in this assessment gives results that are consistent with findings from other studies. As expected, the most robust platform types are also the most expensive, confirming the trade-off between structural resilience and cost. Among the system components, PV panels/modules represent the largest share of the investment, followed by the platform costs. In terms of energy production, Ceuta stands out as the most performant location, achieving 1,563.74 MWh over 20 years, despite the application of seasonal removal (SR) and only 8 months of annual operation. This is primarily due to the high solar irradiance at the site and the use of a tracking system enabled by the Class 1 configuration. In contrast, Gotland records the lowest energy output among the selected locations (856.49 MWh), even though SR is not applied and the system operates year-round. This outcome reflects both the limited solar resource at that latitude and the constraints imposed by the Class 3 configuration, which allows only for fixed horizontal panels without tracking.

Among the selected locations, the highest Net Present Value (NPV) after 20 years is observed in Ceuta and Pantelleria, corresponding to Class 1 and Class 3 systems, respectively. In Ceuta, this is primarily due to the high energy yield (1,563.74 MWh), supported by favorable irradiance conditions and the implementation of a tracking system. In Pantelleria, despite the use of a fixed horizontal panel configuration typical of Class 3 and a slightly lower energy production (1,435.89 MWh), the high local electricity price (0.281 €/kWh) significantly boosts the economic return, resulting in a cumulative NPV of nearly €1.74 million—even with a higher $CapEx$ compared to Ceuta. Ceuta also achieves the fastest payback period, mainly due to the relatively low initial investment required. In contrast, Gotland is not economically viable due to its low energy production and high upfront costs. Jersey, while producing a substantial amount of energy (1,248.67 MWh), shows the lowest NPV among all locations. This is attributed to France's lower electricity prices, which diminish the economic benefit despite decent technical performance.

While the locations that exhibit the highest environmental benefit are those with the greatest amount of CO_2 emissions avoided, the Gulf of Gabès stands out with 939.72 tonnes of CO_2 saved over the system's lifetime. This result is primarily due to the high EF_{grid} of the Tunisian electricity grid, which means that replacing grid electricity with clean PV generation leads to significant CO_2 savings. On the other hand, Gotland shows the lowest environmental impact, with only 269.17 tonnes of CO_2 avoided. This is explained by the already high share of renewable energy in Sweden's grid, resulting in a lower EF_{grid} and consequently a reduced potential for additional CO_2 reductions through photovoltaic deployment.

Table 8.1: LCOE, Cumulative NPV and t_{PBT} for Each Location over 20 Years

Location	**LCOE [€/MWh]**	**Cumulative** NPV **[€]**	$t_{\mathbf{PBT}}$ **[years]**
Ceuta	122.23	1,368,723	7
Gotland	240.06	-302,123	-
Gulf Gabès	133.27	812,920	9
Pantelleria	143.19	1,737,676	8
Zadar	143.82	1,008,612	10
Jersey	153.07	406,231	13

8.3 Techno-Economic Impact of Seasonal Removal Strategies

Another important finding of this study is the introduction of a SR strategy as a design optimization measure. By identifying and excluding the months with the most extreme wave conditions, several sites initially classified under more robust and costly platform categories could be reassigned to lighter structures. Specifically, Ceuta and Jersey were reclassified from Class 3 to Class 1, while the Gulf of Gabes and Zadar shifted from Class 1 to Class 2. This method allows for a significant reduction in structural requirements and capital costs, without compromising safety, by avoiding over-dimensioning for rare and short-lived events. However, this strategy results in a reduction of the annual energy yield. The following figure illustrates the relative share of energy lost due to the SR.

Gotland and Pantelleria show 100% energy exploitation, as no SR is applied. In contrast, the share of directly lost energy due to SR ranges from 22.2% in Zadar to 33.5% in the Gulf of Gabès. These represent only the immediate losses from system deactivation. Additional energy losses occur in locations where platforms are reassigned from Class 1 to Class 2 configurations, due to the absence of a tracking system. Conversely, when moving from Class 3 to Class 1, there is a trade-off: while SR reduces the total available days for energy production, the introduction of a tracking system in Class 1 leads to a significant energy gain. The following figure compares the daily energy production over one year for the four studied locations—Gulf of Gabès, Ceuta, Zadar, and Jersey—highlighting how energy output varies between platform classes and illustrating the combined effects of tracking and SR.

The following Table 8.2 , the total energy losses over a 20-year system lifetime for each location, accounting for an annual PV panel degradation rate of 2%. For each site, it reports the cumulative energy lost due to SR strategies, along

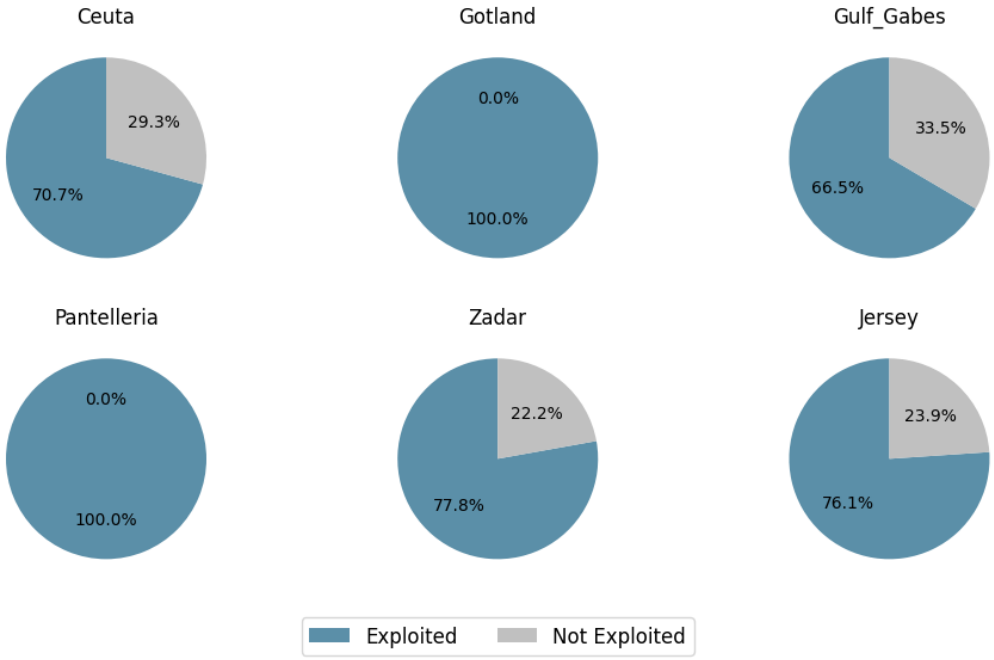

Figure 8.1: Annual share of exploited vs. non-exploited energy due to SR at each location.

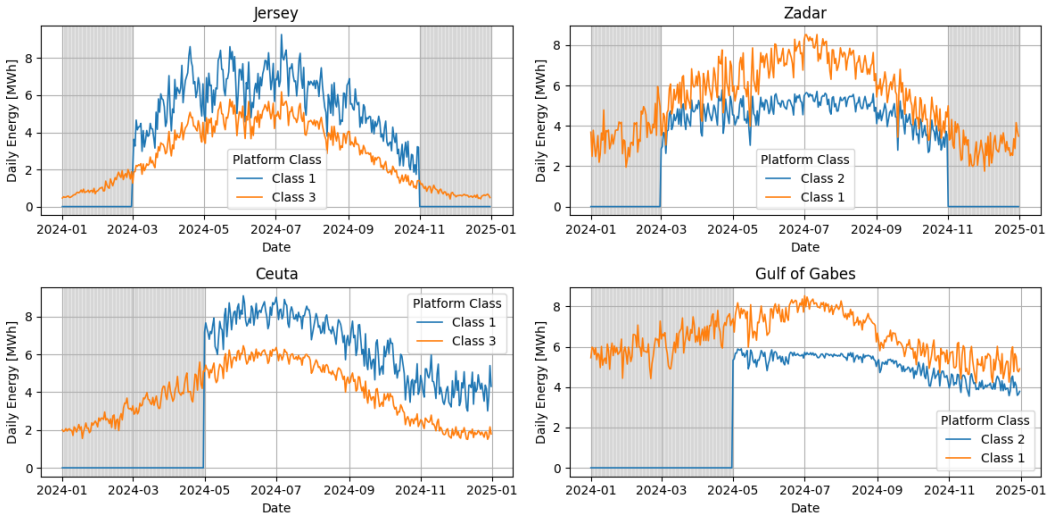

Figure 8.2: Comparison of daily energy production between platform classes for the Gulf of Gabès, Ceuta, Zadar, and Jersey. The plots highlight the impact of SR and the presence or absence of tracking systems on the annual energy yield.

with the corresponding monetary losses calculated using location-specific energy prices. The table also includes estimated $CapEx$ savings resulting from the use of simpler platform classes. However, these savings are offset in some cases by increased $OpEx$, as SR requires dismantling and redeploying the system each year, leading to higher operational expenses. The final column presents the net financial balance, combining all gains and losses to highlight the overall economic impact of implementing SR strategies.

Table 8.2: Lifetime energy and monetary impacts due to SR.

Location	**Energy [MWh]**	**Energy Value Impact [€]**	*CapEx* **[€]**	*OpEx* **[€]**	**Net [€]**
Ceuta	2,634.92	578,983.00	389,000.00	-264,600.00	703,383.00
Gulf Gabès	-18,957.72	-3,954,120.00	265,000.00	-189,000.00	-3,878,120.00
Zadar	-13,355.23	-3,239,198.00	265,000.00	-189,000.00	-3,163,198.00
Jersey	6,160.09	1,158,417.00	389,000.00	-264,600.00	1,282,817.00

For the Table8.2 is evident that SR is not always economically advantageous. In particular, locations like Zadar and Gulf Gabès experience a net negative impact, meaning the combined effect of reduced energy production, increased operational costs, and loss of tracking system benefits outweighs the potential $CapEx$ savings. These cases represent transitions from Class 1 to Class 2 configurations, where the platforms are resticted to have fixed tilt and are also periodically removed from the sea. This leads to both the loss of operational months and the absence of the tracking system, significantly reducing energy output. Conversely, for locations originally categorized as Class 3 and then recategorized to Class 1 with SR, such as Ceuta and Jersey, despite shortening the annual operation window, they still result in a positive net benefit. This is primarily due to the implementation of a tracking system in Class 1, which compensates for the reduced operational time by enhancing energy yield during the active months. These findings suggest that the implementation of SR is most economically beneficial when it allows a location to upgrade from a Class 3 to a Class 1 configuration—where the adoption of a tracking system significantly boosts energy yield. Conversely, applying SR to Class 1 locations to reduce costs by shifting to Class 2 often leads to a net negative impact. Therefore, maintaining a Class 1 setup is generally the most advantageous choice whenever wave conditions already fall within Class 1 thresholds, and SRshould primarily be considered as a strategic upgrade path for Class 3 sites.

Chapter 9

Future Outlook

The DDA has some limits discussed already in Section4, the main one is the use of ERA5 wave height data, with its coarse spatial resolution, which can overlook local effects in nearshore environments. Additionally, the exclusion of dynamic loads such as wind, currents, and wave periods may lead to underestimations in structural requirements. Looking forward, future research could enrich this methodology by integrating multi-parametric environmental data, validating design assumptions through prototype testing, and exploring hybrid configurations or adaptive mooring systems. Such efforts will help further bridge the gap between early feasibility and detailed engineering design, accelerating the deployment of offshore FPV in real-world scenarios.

Chapter 10

Summary

This thesis introduced a replicable and clear methodology for assessing the techno-economic and environmental feasibility of offshore FPV systems across diverse maritime locations. By combining a DDA for the classification based on H_s with a BuA for the $CapEx$ estimation, the study fills a methodological gap in early-stage offshore PV planning. The model described in this study allows a clear comparison of the different platform typologies, highlights the cost-performance trade-offs of structural classes, and supports choosing the best option for each location without needing complex simulations. In Table 10.1 are summarised the final results related to the DDA and BuA are summarised to evaluate the $CapEx$ for the whole FPV system.

Table 10.1: Summary of Classification Results and $CapEx$ Estimates for Each Location Based on the DDA and BuA

Platform Class	**Max H_sm**	**Cost [€/kWp]**
Class 2	1.47	1,383.53
Class 1	2.08	1,619.09
Class 3	4.03	1,928.63

Furthermore, the integration of a SR strategy has been proven to be a valuable tool to adapt system design to site constraints and improve cost-efficiency in marginal locations. Sometimes the SR leads to a shift from more advanced to less flexible platform classes (see the case study of Gulf of Gabes and Zadar); the outcome is often negative due to reduced energy production, higher operational costs, and the loss of tracking capabilities. In contrast, applying SR to reclassify systems from more constrained to more optimized configurations can result in a net benefit, as the introduction of tracking systems boosts energy yields enough

to offset the reduced operational time, as is possible to observe in case study of Ceuta and Jersey, as is possible to see in the results summarised in Table 8.2, where the impact of the SR is analysed for different locations. The results on the environmental impacts demonstrate that FPV systems can substantially reduce tCO_2 emissions, particularly because they are often deployed in semi-isolated areas. These locations typically depend on diesel generators or other high-emission energy sources, leading to elevated EF_{avg}, as shown in Table 7.4. Consequently, replacing a portion of this electricity demand with clean solar energy from FPV installations results in greater tCO_2 savings compared to other RES installed in regions with already decarbonized grids.

Appendix A

Backend Functions of the Parametric Tool

```
def design_function(Class ,capacity, sea_depth):
        modules_per_platform = {
            "Class1": 70,   #for 70 modules
            "Class2": 100,   #for 100 modules
            "Class3": 80   #for 80 modules
        }
        N_modules= capacity*10**3/0.4 #Number of modules
        N_platforms= int(N_modules/modules_per_platform.get(Class,
    None)) #Number of pltaforms
        Chain_Length=sea_depth*1.4 #Total length of one single chain

        return  N_modules, N_platforms,Chain_Length

def mooring_cost_function(Class, Chain_Length, N_platforms):
    N_lines = {
        "Class1": 1,   #for 70 modules
        "Class2": 1,   #for 100 modules
        "Class3": 2   #for 80 modules
    }

    #Cost of the mooring system
    C_chain=Chain_Length*18.2*2.75*N_platforms*N_lines.get(Class,
    None) #Cost Chains
    C_anchors=736000*0.052/9.81*N_platforms*N_lines.get(Class, None)
    #Cost anchors
    Mooring_Cost=(C_chain+C_anchors)

    return  Mooring_Cost
```

```
26
27
28 def platfrom_cost_function(Class, N_platforms):
29
30
31     class_type_mapping = {
32         "Class1": 11366,   #for 70 modules
33         "Class2": 9620,   #for 100 modules
34         "Class3": 16503    #for 80 modules
35     }
36
37     Platfroms_Cost = class_type_mapping.get(Class, None)*N_platforms
38
39     return    Platfroms_Cost
40
41
42 def electrical_cost(Power, distance):
43     #Power in MW
44     #Distance in km
45
46     C_substation=157360*Power
47     C_cables=2.18*Power*distance
48     Panels_Cost=300*10**6*Power/400
49
50     Electrical_cost=C_cables+C_substation
51
52     return    Panels_Cost, Electrical_cost
53
54
55 def labour_cost_function(Mooring_Cost,Platfroms_Cost,Electrical_cost,
       Panels_Cost):
56
57     #Total labour cost, equal to 5% of the total components cost
58     C_labour=(Mooring_Cost+Platfroms_Cost+Electrical_cost+Panels_Cost
       )*0.05
59
60     return    C_labour
61
62
63
64 def OPEX_function(Class, distance,N_platforms,capacity,location):
65     class_type_mapping = {
66         "Class1": 5,   #for 70 modules
67         "Class2": 5,   #for 100 modules
68         "Class3": 2    #for 80 modules
69     }
70
71
72     v_boat=20000 #m/h
```

```
73      c_boat=120 #e/h
74      c_divers=90*4 #e/h 4 divers
75      c_workers=50*3 #e/h i consider 3 workers
76      T_install=0.5 #Time required to install each floating PV
        structure
77
78      if location in ['Ceuta','Jersey', 'Gulf_Gabes','Zadar']:
79          cost_SPR=N_platforms*(T_install+2*distance/v_boat)*(c_boat+
        c_divers+c_workers)/class_type_mapping.get(Class, None)
80      else: cost_SPR=0
81
82      #Yearly opertional Cost equal to $15 for each kw of nominal power
83
84      Opex=(capacity*15*10**3+cost_SPR)/10**3  #result in kEuro
85
86      return Opex
87
88
89
90  def COSTS(Class ,Power, sea_depth, distance):
91      [N_modules, N_platforms,Chain_Length]=design_function(Class ,
        Power, sea_depth)
92      Mooring_Cost=mooring_cost_function(Class, Chain_Length,
        N_platforms)
93      Platfroms_Cost=platfrom_cost_function(Class, N_platforms)
94      [Panels_Cost, Electrical_cost] =electrical_cost(Power, distance)
95      C_labour=labour_cost_function(Mooring_Cost,Platfroms_Cost,
        Electrical_cost,Panels_Cost)
96      return Mooring_Cost, Platfroms_Cost, Panels_Cost, Electrical_cost
        , C_labour
97
98
99  def calculate_lcoe(life_time, capex, opex, production):
100
101     years=list(range(0, life_time))
102     discount_rate=0.06
103     # Calculate discounted OPEX and production
104     discounted_opex = [opex / (1 + discount_rate) ** year for year in
        years]
105     discounted_production = [production / (1 + discount_rate) ** year
        for year, production in zip(years, production)]
106
107     # Exclude the last year for discounted production sum
108     discounted_production_sum = sum(discounted_production[:-1])
109
110     # Calculate LCOE
111     lcoe = (capex + sum(discounted_opex)) / discounted_production_sum
112
113     return lcoe
```

$\mathcal{O}(n \log n)$
`numpy`

Bibliography

[1] Sanja Filipović, Noam Lior, and Mirjana Radovanović. «The green deal – just transition and sustainable development goals Nexus». In: *Renewable and Sustainable Energy Reviews* 168 (2022), p. 112759. ISSN: 1364-0321. DOI: https://doi.org/10.1016/j.rser.2022.112759. URL: https://www.sciencedirect.com/science/article/pii/S136403212200644X (cit. on p. 1).

[2] Paolo Venturini, Gabriele Guglielmo Gagliardi, Giuliano Agati, Luca Cedola, Michele Vincenzo Migliarese Caputi, and Domenico Borello. «Integration of Floating Photovoltaic Panels with an Italian Hydroelectric Power Plant». In: *Energies* 17.4 (2024). ISSN: 1996-1073. URL: https://www.mdpi.com/1996-1073/17/4/851 (cit. on pp. 1, 2, 4).

[3] M. López, F. Soto, and Z.A. Hernández. «Assessment of the potential of floating solar photovoltaic panels in bodies of water in mainland Spain». In: *Journal of Cleaner Production* 340 (2022), p. 130752. ISSN: 0959-6526. DOI: https://doi.org/10.1016/j.jclepro.2022.130752. URL: https://www.sciencedirect.com/science/article/pii/S0959652622003912 (cit. on pp. 1, 2).

[4] Alok Sahu, Neha Yadav, and K. Sudhakar. «Floating photovoltaic power plant: A review». In: *Renewable and Sustainable Energy Reviews* 66 (2016), pp. 815–824. ISSN: 1364-0321. DOI: https://doi.org/10.1016/j.rser.2016.08.051. URL: https://www.sciencedirect.com/science/article/pii/S1364032116304841 (cit. on pp. 1, 4).

[5] Adimas Pradityo Sukarso and Kyung Nam Kim. «Cooling Effect on the Floating Solar PV: Performance and Economic Analysis on the Case of West Java Province in Indonesia». In: *Energies* 13.9 (2020). ISSN: 1996-1073. DOI: 10.3390/en13092126. URL: https://www.mdpi.com/1996-1073/13/9/2126 (cit. on pp. 1, 34).

[6] Christopher Small and Robert J. Nicholls. «A Global Analysis of Human Settlement in Coastal Zones». In: *Journal of Coastal Research* 19.3 (2003),

pp. 584–599. ISSN: 07490208, 15515036. URL: http://www.jstor.org/stable/4299200 (visited on 04/23/2025) (cit. on p. 1).

[7] Sara Oliveira-Pinto and Jasper Stokkermans. «Assessment of the potential of different floating solar technologies – Overview and analysis of different case studies». In: *Energy Conversion and Management* 211 (2020), p. 112747. ISSN: 0196-8904. DOI: https://doi.org/10.1016/j.enconman.2020.112747. URL: https://www.sciencedirect.com/science/article/pii/S0196890420302855 (cit. on pp. 2, 6, 47).

[8] Shiva Gorjian, H. Sharon, Hossein Ebadi, Karunesh Kant, Fausto Bontempo Scavo, and Giuseppe Marco Tina. «Recent technical advancements, economics and environmental impacts of floating photovoltaic solar energy conversion systems». In: *Journal of Cleaner Production* 278 (2021), p. 124285. ISSN: 0959-6526. DOI: https://doi.org/10.1016/j.jclepro.2020.124285. URL: https://www.sciencedirect.com/science/article/pii/S0959652620343304 (cit. on p. 2).

[9] Alberto Ghigo, Emilio Faraggiana, Massimo Sirigu, Giuliana Mattiazzo, and Giovanni Bracco. «Design and Analysis of a Floating Photovoltaic System for Offshore Installation: The Case Study of Lampedusa». In: *Energies* 15.23 (2022). ISSN: 1996-1073. DOI: 10.3390/en15238804. URL: https://www.mdpi.com/1996-1073/15/23/8804 (cit. on pp. 2, 5–7, 37, 40, 42–45).

[10] R. Claus and M. López. «Key issues in the design of floating photovoltaic structures for the marine environment». In: *Renewable and Sustainable Energy Reviews* 164 (2022), p. 112502. ISSN: 1364-0321. DOI: https://doi.org/10.1016/j.rser.2022.112502. URL: https://www.sciencedirect.com/science/article/pii/S1364032122004063 (cit. on pp. 4–9, 38).

[11] Paul Rappaport. «The photovoltaic effect and its utilization». In: *Solar Energy* 3.4 (1959), pp. 8–18. ISSN: 0038-092X. DOI: https://doi.org/10.1016/0038-092X(59)90002-7. URL: https://www.sciencedirect.com/science/article/pii/0038092X59900027 (cit. on p. 5).

[12] Kim Trapani and Dean L. Millar. «The thin film flexible floating PV (T3F-PV) array: The concept and development of the prototype». In: *Renewable Energy* 71 (2014), pp. 43–50. ISSN: 0960-1481. DOI: https://doi.org/10.1016/j.renene.2014.05.007. URL: https://www.sciencedirect.com/science/article/pii/S0960148114002584 (cit. on p. 5).

[13] Sara Oliveira-Pinto and Jasper Stokkermans. «Marine floating solar plants: an overview of potential, challenges and feasibility». In: *Proceedings of the Institution of Civil Engineers - Maritime Engineering* 173.4 (2020), pp. 120–135. ISSN: 1741-7597. DOI: https://doi.org/10.1680/jmaen.2020.10. URL:

https://www.sciencedirect.com/science/article/pii/S1741759720000110 (cit. on p. 5).

[14] Balázs Endrődi, Cintia Alexandra Trapp, István Szén, Imre Bakos, Miklós Lukovics, and Csaba Janáky. «Challenges and Opportunities of the Dynamic Operation of PEM Water Electrolyzers». In: *Energies* 18.9 (2025). ISSN: 1996-1073. DOI: 10.3390/en18092154. URL: https://www.mdpi.com/1996-1073/18/9/2154 (cit. on pp. 5, 7–9, 24).

[15] Hesan Ziar, Bjorn Prudon, Fen-Yu Lin, and Bart Roeffen. «Innovative Floating Bifacial Photovoltaic Solutions for Inland Water Areas». In: *Progress in Photovoltaics* 29.7 (2020). URL: https://www.mdpi.com/1996-1073/18/9/2154 (cit. on p. 5).

[16] Swati S Gurfude and P S Kulkarni. «Energy Yield of Tracking Type Floating Solar PV Plant». In: *2019 National Power Electronics Conference (NPEC)*. 2019, pp. 1–6. DOI: 10.1109/NPEC47332.2019.9034846 (cit. on p. 5).

[17] Giuseppe Marco Tina, Fausto Bontempo Scavo, Leonardo Micheli, and Marco Rosa-Clot. «Economic comparison of floating photovoltaic systems with tracking systems and active cooling in a Mediterranean water basin». In: *Energy for Sustainable Development* 76 (2023), p. 101283. ISSN: 0973-0826. DOI: https://doi.org/10.1016/j.esd.2023.101283. URL: https://www.sciencedirect.com/science/article/pii/S0973082623001400 (cit. on p. 5).

[18] A. Martinez and G. Iglesias. «Mapping of the levelised cost of energy from floating solar PV in coastal waters of the European Atlantic, North Sea and Baltic Sea». In: *Solar Energy* 279 (2024), p. 112809. ISSN: 0038-092X. DOI: https://doi.org/10.1016/j.solener.2024.112809. URL: https://www.sciencedirect.com/science/article/pii/S0038092X24005048 (cit. on pp. 6, 44, 47, 48).

[19] Pietro Elia Campana, Louise Wästhage, Worrada Nookuea, Yuting Tan, and Jinyue Yan. «Optimization and assessment of floating and floating-tracking PV systems integrated in on- and off-grid hybrid energy systems». In: *Solar Energy* 177 (2019), pp. 782–795. ISSN: 0038-092X. DOI: https://doi.org/10.1016/j.solener.2018.11.045. URL: https://www.sciencedirect.com/science/article/pii/S0038092X18311459 (cit. on p. 6).

[20] DNV GL AS. *Recommended Practice DNVGL-RP-0584: Design, Development and Operation of Floating Solar Photovoltaic Systems*. Technical Report. DNV GL AS, 2021 (cit. on p. 7).

[21] Sun-Hee Kim, Seung-Cheol Baek, Ki-Bong Choi, and Sung-Jin Park. «Design and Installation of 500-kW Floating Photovoltaic Structures Using High-Durability Steel». In: *Energies* 13.19 (2020). ISSN: 1996-1073. DOI: 10.3390/en13194996. URL: https://www.mdpi.com/1996-1073/13/19/4996 (cit. on p. 8).

[22] Ciel & Terre. *Hydrelio®: the patented floating PV system*. https://www.ciel-et-terre.net/hydrelio-floating-solar-technology/hydrelio-products/. Accessed: 2025-04-24. 2011 (cit. on pp. 8, 39).

[23] E. Bellini. *Floating PV in the Persian Gulf*. https://www.pv-magazine.com/2020/02/17/floating-pv-in-the-persian-gulf/. PV Magazine, Accessed: 2025-04-24. 2020 (cit. on p. 8).

[24] J. Scully. *Chenya Energy eyes floating PV growth after completing 181MWp offshore project*. https://www.pv-tech.org/chenya-energy-eyes-floating-pv-growth-after-completing-181mwp-offshore-project. PV Tech, Accessed: 2025-04-24. 2021 (cit. on p. 8).

[25] Oceans of Energy. *North Sea 1 Offshore Solar Project*. https://oceansofenergy.blue/north-sea-1-/. Accessed: 2025-04-24. 2025 (cit. on p. 9).

[26] K. N. Sheeba, R. Madhusudhana Rao, and S. Jaisankar and. «A Study on the Underwater Performance of a Solar Photovoltaic Panel». In: *Energy Sources, Part A: Recovery, Utilization, and Environmental Effects* 37.14 (2015), pp. 1505–1512. DOI: 10.1080/15567036.2011.619632. eprint: https://doi.org/10.1080/15567036.2011.619632. URL: https://doi.org/10.1080/15567036.2011.619632 (cit. on p. 9).

[27] Kim Trapani and Dean L. Millar. «The thin film flexible floating PV (T3F-PV) array: The concept and development of the prototype». In: *Renewable Energy* 71 (2014), pp. 43–50. ISSN: 0960-1481. DOI: https://doi.org/10.1016/j.renene.2014.05.007. URL: https://www.sciencedirect.com/science/article/pii/S0960148114002584 (cit. on p. 9).

[28] Ocean Sun AS. *Ocean Sun: Towards a Clean Energy Future*. https://oceansun.no/. Accessed: 2025-04-24. 2025 (cit. on p. 9).

[29] P. Sánchez Molina and E. Bellini. *CIGS Solar Panels for Offshore PV*. https://www.pv-magazine.com/2021/12/01/cigs-solar-panels-for-offshore-pv/. PV Magazine, Accessed: 2025-04-24. 2021 (cit. on p. 9).

[30] David Firnando Silalahi and Andrew Blakers. «Global Atlas of Marine Floating Solar PV Potential». In: *Solar* 3.3 (2023), pp. 416–433. ISSN: 2673-9941. DOI: 10.3390/solar3030023. URL: https://www.mdpi.com/2673-9941/3/3/23 (cit. on pp. 10, 11).

[31] In: (). URL: https://www.ecmwf.int/en/forecasts/dataset/ecmwf-reanalysis-v5 (cit. on pp. 10, 23).

[32] Francesco Barbariol, Silvio Davison, Francesco Marcello Falcieri, Rossella Ferretti, Antonio Ricchi, Mauro Sclavo, and Alvise Benetazzo. «Wind Waves in the Mediterranean Sea: An ERA5 Reanalysis Wind-Based Climatology». In: *Frontiers in Marine Science* Volume 8 - 2021 (2021). ISSN: 2296-7745. DOI: 10.3389/fmars.2021.760614. URL: https://www.frontiersin.org/journals/marine-science/articles/10.3389/fmars.2021.760614 (cit. on pp. 10–12).

[33] EMODnet. *EMODnet Bathymetry Viewer*. Accessed: 2025-04-24. 2025. URL: https://emodnet.ec.europa.eu/geoviewer/ (cit. on pp. 13, 16).

[34] C Montero. «Solutions for electricity provision in the off-grid autonomous city of Ceuta (Spain)». In: *Master. university of Strathclyde* (2018) (cit. on p. 14).

[35] OpenStreetMap contributors. *OpenStreetMap*. https://www.openstreetmap.org. Accessed: 2025-06-29. 2025 (cit. on pp. 14, 15, 17–19).

[36] Miquel Àngel Martínez-Medina, Miguel Ángel Pérez-Martín, and Teodoro Estrela. «Desalination in Spain and the Role of Solar Photovoltaic Energy». In: *Journal of Marine Science and Engineering* 12.6 (2024). ISSN: 2077-1312. URL: https://www.mdpi.com/2077-1312/12/6/859 (cit. on p. 15).

[37] Daniele Mosso, Luca Rajteri, and Laura Savoldi. «Integration of Land Use Potential in Energy System Optimization Models at Regional Scale: The Pantelleria Island Case Study». In: *Sustainability* 16.4 (2024), p. 1644 (cit. on p. 15).

[38] Riccardo Novo, Francesco Demetrio Minuto, Giovanni Bracco, Giuliana Mattiazzo, Romano Borchiellini, and Andrea Lanzini. «Supporting decarbonization strategies of local energy systems by de-risking investments in renewables: a case study on pantelleria island». In: *Energies* 15.3 (2022), p. 1103 (cit. on pp. 15, 16).

[39] Regione Siciliana - Dipartimento dell'Acqua e dei Rifiuti. *Relazione Tecnica: Impianto di Dissalazione a Pantelleria*. Accessed: 2025-07-01. 2013. URL: https://pti.regione.sicilia.it/portal/page/portal/PIR_PORTALE/PIR_LaStrutturaRegionale/PIR_AssEnergia/PIR_Dipartimentodellacquaedeirifiuti/PIR_Bandi/PIR_20131118IMPIANTODISSALAZIONEPANTELLERIA/Relazione%20Dissalatore%20Pantelleria.pdf (cit. on p. 16).

[40] Paola Badurina, Marijan Cukrov, and Čedomir Dundović. «Contribution to the implementation of "Green Port" concept in Croatian seaports». In: *Pomorstvo* 31.1 (2017), pp. 10–17 (cit. on pp. 16, 17).

[41] Faten Attig-Bahar, Uwe Ritschel, Peter Akari, Ibrahim Abdeljelil, and Mahbouba Amairi. «Wind energy deployment in Tunisia: Status, Drivers, Barriers and Research gaps—A Comprehensive review». In: *Energy Reports* 7 (2021), pp. 7374–7389. ISSN: 2352-4847. DOI: https://doi.org/10.1016/j.egyr.2021.10.087. URL: https://www.sciencedirect.com/science/article/pii/S2352484721011057 (cit. on p. 18).

[42] Roukaya Issaoui, Christine Rösch, Jörg Woidasky, Mario Schmidt, and Tobias Viere. «Cradle-to-gate life cycle assessment of beneficiated phosphate rock production in Tunisia [Ökobilanz der Produktion von aufbereitetem Phosphatgestein in Tunesien (von der Wiege bis zu Bahre)]». In: *Sustainability Nexus Forum* 29.2 (June 2021), pp. 107–118. DOI: 10.1007/s00550-021-00522-8. URL: https://ideas.repec.org/a/spr/sumafo/v29y2021i2d10.1007_s00550-021-00522-8.html (cit. on p. 18).

[43] Khaoula Daghsen, Dorra Lounissi, and Nahla Bouaziz. «A universal model for solar radiation exergy accounting: Case study of Tunisia». In: *Archives of Thermodynamics* (2022), pp. 97–118 (cit. on p. 18).

[44] Sam Cross, Behnam Zakeri, David Padfield, and Sanna Syri. «Is battery energy storage economic in islanded power systems? Focus on the island of Jersey». In: *2016 13th International Conference on the European Energy Market (EEM)*. 2016, pp. 1–5. DOI: 10.1109/EEM.2016.7521219 (cit. on pp. 19, 20).

[45] Johan Lindahl et al. «National survey report of PV power applications in Sweden». In: *Uppsala University and International Energy Agency: Uppsala, Sweden* 9 (2014) (cit. on p. 20).

[46] In: (). URL: https://solargis.com/maps-and-gis-data/download/sweden (cit. on p. 20).

[47] Jennifer Leijon, Jens Engström, Malin Göteman, and Cecilia Boström. «Desalination and wave power for freshwater supply on Gotland». In: *Energy Strategy Reviews* 53 (2024), p. 101404 (cit. on p. 21).

[48] Yunus Doğan and Ahmet Durap. «Summarizing data sets for data mining by using statistical methods in coastal engineering». In: *World Academ Sci Eng Technol Int J Comput Inform Eng* 11 (2017), pp. 643–648 (cit. on p. 22).

[49] European Commission. *Photovoltaic Geographical Information System (PVGIS)*. Accessed: 2025-04-24. 2025. URL: https://ec.europa.eu/jrc/en/pvgis (cit. on p. 30).

[50] Enrico Giglio, Ermando Petracca, Bruno Paduano, Claudio Moscoloni, Giuseppe Giorgi, and Sergej Antonello Sirigu. «Estimating the Cost of Wave Energy Converters at an Early Design Stage: A Bottom-Up Approach». In: *Sustainability* 15.8 (2023). ISSN: 2071-1050. DOI: 10.3390/su15086756. URL: https://www.mdpi.com/2071-1050/15/8/6756 (cit. on p. 37).

[51] In: (). URL: https://solarduck.tech/ (cit. on pp. 40, 41).

[52] In: (). URL: https://www.hydro.com/en/en/ (cit. on p. 41).

[53] Gobind Pillai and Husain Ali Yaqoob Naser. «Techno-economic potential of largescale photovoltaics in Bahrain». In: *Sustainable Energy Technologies and Assessments* 27 (2018), pp. 40–45. ISSN: 2213-1388. DOI: https://doi.org/10.1016/j.seta.2018.03.003. URL: https://www.sciencedirect.com/science/article/pii/S2213138817303703 (cit. on pp. 45, 47).

[54] Daniel Soto. «Modeling and measurement of specific fuel consumption in diesel microgrids in Papua, Indonesia». In: *Energy for Sustainable Development* 45 (2018), pp. 180–185. ISSN: 0973-0826. DOI: https://doi.org/10.1016/j.esd.2018.06.013. URL: https://www.sciencedirect.com/science/article/pii/S0973082618307403 (cit. on p. 46).

[55] In: (). URL: https://www.globalpetrolprices.com/diesel_prices/ (cit. on p. 46).

[56] In: (). URL: https://www.voronoiapp.com/energy/Whats-the-Average-Cost-of-1-kWh-Electricity-around-the-World--3398 (cit. on p. 46).

[57] In: (). URL: https://euenergy.live/ (cit. on p. 46).

[58] Enrico Giglio, Ermando Petracca, Bruno Paduano, Claudio Moscoloni, Giuseppe Giorgi, and Sergej Antonello Sirigu. «Estimating the Cost of Wave Energy Converters at an Early Design Stage: A Bottom-Up Approach». In: *Sustainability* 15.8 (2023). ISSN: 2071-1050. DOI: 10.3390/su15086756. URL: https://www.mdpi.com/2071-1050/15/8/6756 (cit. on p. 48).

[59] In: (). URL: https://ourworldindata.org/grapher/carbon-intensity-electricity (cit. on p. 52).

[60] Abdul Qayoom Jakhrani, Andrew Ragai Henry Rigit, Al-Khalid Othman, Saleem Raza Samo, and Shakeel Ahmed Kamboh. «Estimation of carbon footprints from diesel generator emissions». In: *2012 International Conference on Green and Ubiquitous Technology*. 2012, pp. 78–81. DOI: 10.1109/GUT.2012.6344193 (cit. on p. 52).